DALHOUSIE UNIVERSITY

QUANTIFYING IMPACTS OF SPATIAL RESOLUTION ON PIXEL AND OBJECT-BASED METHODS OF IMAGE CLASSIFICATION: A CASE STUDY OF IDENTIFYING ESTUARINE MORPHOLOGY IN COBEQUID BAY, NOVA SCOTIA, CANADA

Bay Berry

SUBMITTED IN PARTIAL FULFILMENT OF THE REQUIREMENTS FOR THE DEGREE OF BACHELOR OF SCIENCES, HONOURS

DEPARTMENT OF EARTH AND ENVIRONMENTAL SCIENCES

DALHOUSIE UNIVERSITY, HALIFAX, NOVA SCOTIA

April 2020

DALHOUSIE UNIVERSITY

Department of Earth Sciences
Halifax, Nova Scotia
Canada B3H 4R2
(902) 494-2358

DATE: 03/30/2020

AUTHOR: Bay Berry

TITLE: Quantifying impacts of spatial resolution on pixel and object-based methods of image classification: A case study of identifying estuarine morphology in Cobequid Bay, Nova Scotia, Canada

DEGREE: B.Sc. Earth Sciences CONVOCATION: May YEAR: 2020

Distribution License

DalSpace requires agreement to this non-exclusive distribution license before your item can appear on DalSpace.

NON-EXCLUSIVE DISTRIBUTION LICENSE

You (the author(s) or copyright owner) grant to Dalhousie University the non-exclusive right to reproduce and distribute your submission worldwide in any medium.

You agree that Dalhousie University may, without changing the content, reformat the submission for the purpose of preservation.

You also agree that Dalhousie University may keep more than one copy of this submission for purposes of security, back-up and preservation.

You agree that the submission is your original work, and that you have the right to grant the rights contained in this license. You also agree that your submission does not, to the best of your knowledge, infringe upon anyone's copyright.

If the submission contains material for which you do not hold copyright, you agree that you have obtained the unrestricted permission of the copyright owner to grant Dalhousie University the rights required by this license, and that such third-party owned material is clearly identified and acknowledged within the text or content of the submission.

If the submission is based upon work that has been sponsored or supported by an agency or organization other than Dalhousie University, you assert that you have fulfilled any right of review or other obligations required by such contract or agreement.

Dalhousie University will clearly identify your name(s) as the author(s) or owner(s) of the submission, and will not make any alteration to the content of the files that you have submitted.

If you have questions regarding this license please contact the repository manager at dalspace@dal.ca.

Grant the distribution license by signing and dating below.

Bay Berry	03/30/2020
Name of signatory	Date

Table of contents

List of figures

List of tables

Abstract

Image processing methods can be used to classify land cover and phenomena from satellite imagery according to their spectral characteristics and identify target features. These methods can provide a relatively efficient approach to processing many images and to measuring change of features over time. Selecting an appropriate data source and classification method, however, requires considerations such as the scale of the process under investigation, spectral differences between target areas and their surroundings, and technical limitations for the analyst. The Salmon River estuary within Cobequid Bay, Nova Scotia was chosen to evaluate the impact of spatial resolution on the use of satellite imagery to identify tidal bars. Images were acquired from four satellite systems (PlanetScope, RapidEye, Sentinel-2, Landsat-5) representing a range of spatial resolutions (3m to 30m). Both traditional pixel-based methods (i.e., supervised, unsupervised classification), and object-based image classification methods were used to identify sediment bars within the estuary, and then assessed for classification accuracy. All image types could be classified to at least 80% overall accuracy with a Cohen's Kappa coefficient of 0.9 using at least one method. The research identified trends related to classification result and increasing spatial resolution including: 1) decreasing reliability of unsupervised classification; 2) increased single-pixel errors in supervised classifications, despite overall product reliability; and 3) formation of increasingly meaningful pixel groupings for object-based analysis. Differences in appropriate classification method are considered to be a result of the relationship between scale of phenomenon being mapped and the spatial resolution at which it is represented; when increasing spatial resolution, there is a shift away from presence of mixed-pixels towards the dominance of multi-pixel objects, the classification of which is better suited to object-based as opposed to pixel-based methods. The results suggest a Modifiable Areal Unit Problem-based framework to consider large pixels and object created from small pixels each as viable areal units of analysis for processes at this scale.

Keywords: Remote sensing, scale issue, estuary, geomorphology, Bay of Fundy

Acknowledgements

I would first like to thank my supervisor Dr. Christopher Greene for his guidance and encouragement—over the course of this entire degree, but especially towards the end (Full send!). I would also like to thank the honours coordinator, Dr. Djordje Grujic, for the feedback throughout the year. Thank you to Dr. Lawrence Plug, for agreeing to act as a reader and for providing helpful comments on this final version. Finally, thank you to the members of the Earth and Environmental Sciences Department, for the moral support through this process.

Chapter 1. Introduction

1.1 Introduction

Remote sensing provides a method of mapping features and characteristics of the Earth's surface without the full cost or time associated with repeated ground surveys. Satellite imagery can provide measurements with temporal frequency on the order of weeks or days, depending on the collection system and environmental conditions.

Traditional methods of automated image classification are primarily based on statistical grouping of pixel values. These methods were developed for what could be described as medium to coarse resolution imagery, where a pixel represents an area on the order of tens (10^1) to thousands (10^3) of metres. More readily available high-resolution remote sensing (5m to sub-metre), however, has led to development of methods to handle more detailed, noisy, data-heavy images. The greater availability of images at a wider range of resolutions, coupled with a growing suite of methods to classify the imagery, leads to user uncertainty and may promote ad-hoc strategies to image and classification method selection.

The goal of this project is to investigate the direct influence of spatial resolution in generating an accurate image classification by traditional and more recent methods. The example of estuarine morphology in Cobequid Bay, Nova Scotia, is used here to demonstrate differences related to spatial resolution and methods of classifying remote sensor data. Specifically, satellite imagery collected at a range of spatial resolutions (3m to 30m) were selected from systems measuring energy from similar parts of the electromagnetic spectrum to classify features in the target study area (targeting differences between the channel waters and sediment bars). Ultimately, I seek to answer the following questions: 1) is there a critical threshold at which the ratio between scales of process and data become too great to reliably identify estuarine features; and 2) is this relationship method-dependent?

1.2 Rationale: Choice of setting

The Bay of Fundy, and more specifically Cobequid Bay, provides an interesting setting for this line of investigation for several environmental reasons that pose challenges to remote sensing methods. As described by Rainey and colleagues (2000), macrotidal conditions and low-visibility weather conditions common to maritime settings frequently limit the visibility of intertidal features to a few fortuitous instances when clear skies, low tide, and orbital path of the collection system coincide. When visible, the extent of the intertidal sand bars in Cobequid Bay is quite dramatic—the exposed surface area can be on the order of 1 to 10 km^2 at low tide, while being completely submerged at high tide. However, Amos and Long (1980) also note that the suspended sediment concentration is highest at low water (coincidently, also the ideal time to see sediment bars, and contributing to interest in this problem).

1.3 Scale issues, part 1: Moving from process to data

The word *scale* is used in a range of contexts, and a number of conceptual models have been proposed to define the term. Cao and Lam (1997) suggest four separate definitions, for cartographic, geographic, operational, and measurement scales. Alternatively, scale could be defined in terms of the absolute and relative representations of space (Meentemeyer 1989; Marceau 1999). Scale can also be thought of as the frequency of observation or "window of perception" (Marceau and Hay 1999) by which the world is described. In the context of remote sensing, the frequency of observation and thus scale of the data is defined by the system (on geospatial, temporal, radiometric, and spectral levels—further discussed in section 2.3.2).

As described by Marceau (1999), the *scale issue* refers to challenges posed to spatial analysis relating to the scale of the analytical components. There are two main questions that comprise the scale issue: 1) what is the appropriate scale of study for a given phenomenon; and 2) how can information be adequately transferred between scales?

The perceived scale of the target phenomenon (the scope of an analysis) should inform the resolution of the image data that is used to describe it. Recording a dataset inherently subsets the real-world phenomenon to the level of detail recorded, and from the point of observation onwards our analysis is limited in its detail to the scale of the data (McCarty et al. 1956). Because observations are essentially sub-samples of the "population" (or the real-life phenomenon in its entirety), there is a simplification or generalization associated with recording data (Figure 1). The degree of generalization that is tolerable (or in some cases, most desirable) to the researcher depends on the scale to which they want to describe a phenomenon.

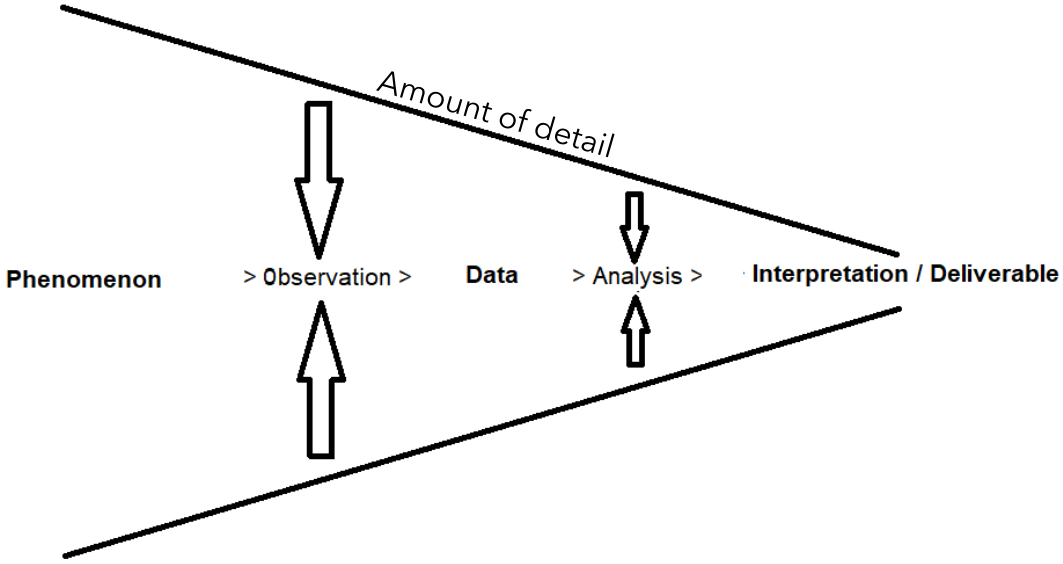

Figure 1. Conceptual model of loss of information at each step of description; generalization occurs at every step where information moves from one dimensionality to the next.

In this example, the estuarine morphology of Cobequid Bay comprises a network of phenomena at a range of perceptible scales. Potential targets and phenomena for study include:

- Overall changes to the basin—the basin is the entity of investigation, and sub-basin level features are ignored

- Changes to sand bar (and inferred scour channel) positions—the components of the system are bars and water, and the bars are treated as whole, homogenous entities

- Finer-scale sedimentary features, such as the ripples on the bar surfaces

Any or all of these levels of investigation could be useful to describe processes of erosion and sedimentation in Cobequid Bay, however each would necessitate a different scale of image data to properly execute automated classification methods to meet minimum accuracy standards. The choice of how we resolve these data, and subsequently how we process them to adequately describe a phenomenon, is the overarching question for this project.

We can inarguably have data that is too coarse for a target process or phenomenon. If the sampling is too infrequent to detect a target phenomenon, then the analytical results cannot be used to create a meaningful description of changes through time and space. While there is certainly a lower limit of spatial resolution where we cannot confidently make a good product, the question I seek to address is converse to this idea: can the spatial resolution of the data be too fine? How does the relationship between scale of process and scale of data affect accuracy? This study addresses this by holding the scale of process constant—looking at tidal bars in an estuarine setting—and varying the spatial resolution of the satellite imagery used to identify them.

Chapter 2. Background

2.1 Study area

This investigation focuses on Cobequid Bay, the eastern inlet of the Minas Basin, Nova Scotia (see Figure 2). I focused on the Salmon River estuary, from 45.36°N, 63.38°W and encompassing the basin area as far as 25 km to the west, where availability of satellite imagery permitted.

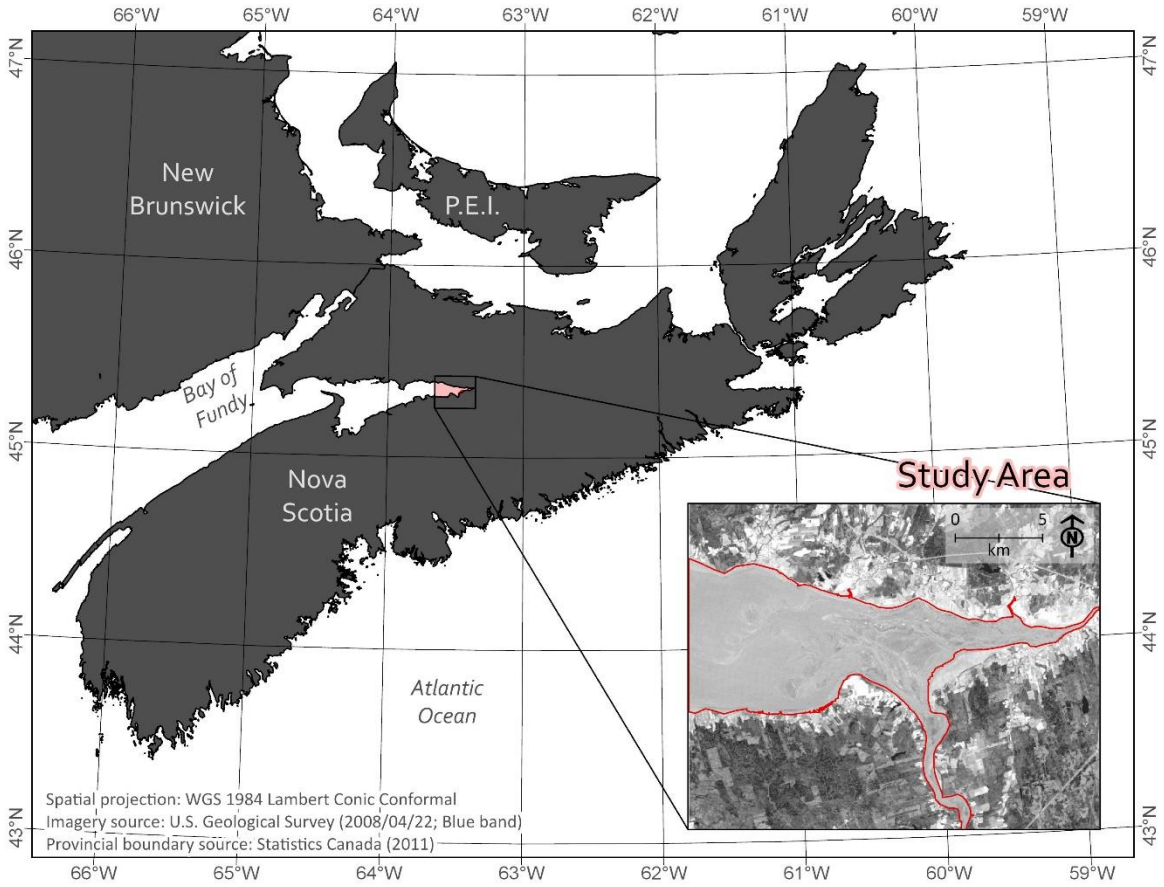

Figure 2. Geographic location of the study area in Cobequid Bay, Nova Scotia, Canada.

Cobequid Bay meets the broad definition of a macrotidal environment; in 2019, the maximum tidal range logged in the area was 16.1m (Burntcoat Head, September 30th 2019; CHS 2019). Tidal scour channels towards the north and south of the bay have gravel and cobbles at their thalwegs. The channels are separated by intertidal flats comprised primarily of sand (Amos and Long 1980).

The net sediment transport direction within Cobequid Bay is east-northeast with sediment derived from four main sources: the cliffs bounding the basin; discharge from the rivers into the estuary; tidal volume of the Bay of Fundy; and seabed reworking (Amos and Long 1980). The erosive cliffs are chiefly Wisconsinan till—primarily local and distally-derived silt, with few areas of gravel and sand meltout till and glaciomarine deposits (Stea et al. 1992). The Salmon River itself discharges an average of 21.6 tonnes of sediment over a complete tidal cycle, from a catchment area of 363 km^2 (Amos and Long 1980). The flood tide also acts as the dominant mechanism of sediment transport, and the intertidal bars tend to migrate eastward (Crewe et al. 2005). When compared to other regions of the Bay of Fundy at the same point in the tidal cycle, Cobequid Bay has recorded notably high suspended sediment content with surface concentrations 10 to 50 times greater than measured in the central Minas Basin (Amos and Long 1980).

2.2 Image classification

2.2.1 In general terms …

Image analysis was developed first for aerial photographs, and later applied to digital images, as a means of supplementing and automating visual interpretation (Blaschke et al. 2014). The traditional approach is pixel-based, meaning that pixel values are considered as individual data points. While enhancements can be applied to integrate spatial patterns and neighbourhood relationships to the classification input, this technique still relies on a cell-by-cell analysis of a raster dataset. Object-based image analysis (or OBIA), which uses descriptive spectral and geometric statistics for pixel clusters instead of their individual values, was developed more recently in response to challenges related to processing high spatial resolution imagery (Blaschke et al. 2000; Benz 2007).

Image classification is the umbrella term for a suite of predictive techniques that use characteristics of a digital image to distinguish features types, or *classes* (Jensen 2005c; Hastie et al. 2009a). These techniques are tools to supplement visual interpretation of an image using a classifying algorithm which, through some series of

statistical decisions and parametrization by the user, assigns areas within the image to a class. The computer system that produces a classified output (referred to as the "classifier") and the person operating the system (referred to as the "user") can work together through three major pathways which are discussed in detail in the following sections.

Before continuing, an important distinction must be made between the terms *spectral class* and *informational class*, as they are not only critical parts of the classification process, but are also managed differently depending on the type of classification being performed. As discussed by Jensen (2005c), a spectral class is a grouping of pixels in multispectral space as interpreted by the classifier (often a software package) as a distribution of numbers, definable by descriptive statistics. In contrast, an informational class relates to how this group of spectrally similar pixels is interpreted by the user, and is usually defined by the colour and shape, land cover and land use, in a way that is meaningful to a person. For this study, two non-hierarchical, mutually exclusive informational classes were identified as *bar* and *water*, as described in Table 1.

Table 1. Informational class descriptions applied in the classifications of the Cobequid Bay study area

Informational class	Description
Bar	Deposited sediment; can be saturated, but not suspended.
Water	Includes clear water (rare) and water with suspended sediment, in channels and pools within the basin area.

2.2.2 Unsupervised pixel-based classification

The first—and arguably the simplest—method of image classification is an unsupervised pixel-based classification (or simply an *unsupervised classification*). In the broadest terms, this method allows the classifier (i.e., the software) to identify natural clusters of pixel values in multispectral space, which are used to define discrete spectral classes (Liu and Mason 2016). Once the classifier assigns each pixel within the image to a spectral class, the user evaluates the results as a post-

classification analysis and assigns an informational class to each spectral class based on their interpretation of the land cover that is represented. Multiple spectral classes can be included ("aggregated") in the same informational class. This method is "pixel-based" in the sense that the numerical value(s) of each pixel is considered independently of the rest of the image. That is, each individual cell of the input raster is tested for membership to a class based only on its own value and does not explicitly consider the values of any neighbouring pixels.

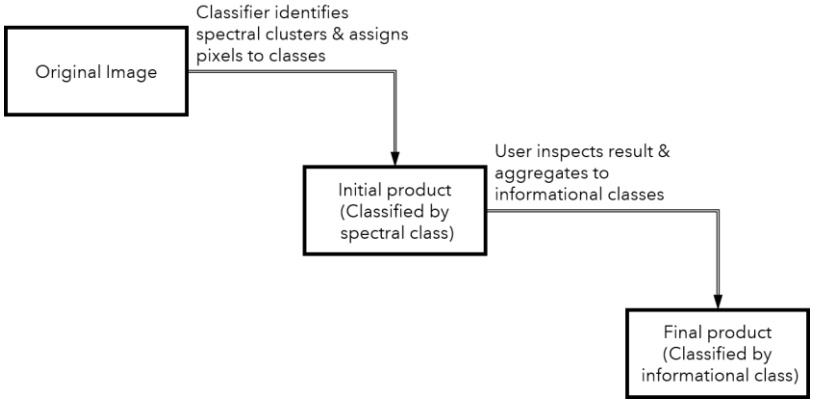

Figure 3. Simplified workflow of a traditional unsupervised classification of multispectral remote sensor data.

2.2.3 Supervised pixel-based classification

A supervised pixel-based classification (or simply a *supervised classification*) differs from the unsupervised classification method in the order of operations of assigning spectral and informational classes to pixels (Liu and Mason 2016). Rather than allowing the classifier to identify spectral clusters, the user instead selects training areas within the image which are representative of the specific informational classes to be classified and extracted from the image. The values of the pixels within these areas are subsequently used to create the statistical definitions of the spectral classes, which are then used to classify the rest of the image on a cell-by-cell basis.

This method is often iterative, where the user may inspect the results of the classification and modify the training areas (in turn modifying the spectral definition of the classes, or *spectral signatures*) in the hope of producing an improved classification result. Potential modifications of training areas may include:

1. Ensuring that pixels have not been incorrectly assigned to training data for a class to which they do not belong;

2. Increasing the number of training areas so that the statistical distribution is more representative of the informational class;

3. Splitting an informational class into two, where the signal appears to be bimodal or otherwise mixed; and

4. Combining two informational classes into one, in the situation where they are spectrally similar enough to be confused by the classifier.

Similar to the unsupervised approach, supervised classification is also a pixel-based method, and only the values of individual pixels of the input raster datasets are considered in the definition of, and assignment to, spectral classes.

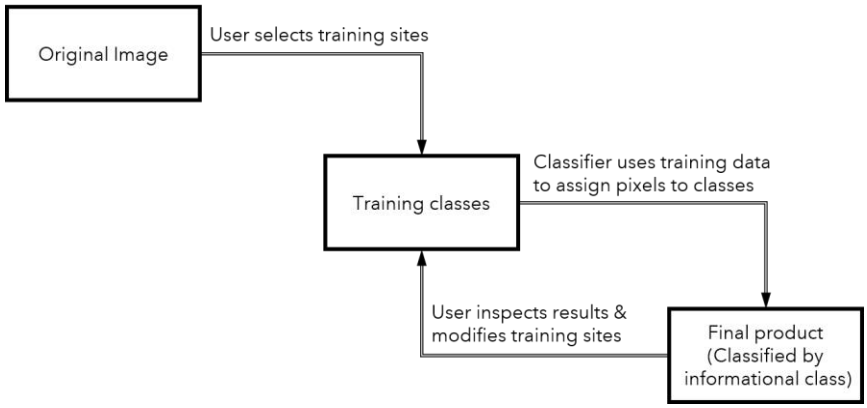

Figure 4. Simplified workflow of a traditional supervised classification of multispectral remote sensor data.

2.2.4 Object-based image analysis

Object-based image analysis is a combination method of unsupervised pixel clustering (*segmentation*) followed by subsequent supervised classification of those clusters (or objects). Image segmentation is not a novel technique, but only in the last two decades has it been streamlined into image classification for geospatial applications (Blaschke et al. 2004). Object-based image analyses originated with the software known as "eCognition" (later "Definiens"; see Benz et al. 2004; Lang and

Tiede 2007), and has since become a popular approach to image classification for remote sensor data (Blaschke 2010). One goal of this object-based approach was to eliminate what Blaschke and colleagues (2000) refer to as the "salt and pepper effect," or sparse single-pixel classification errors.

Instead of considering each individual pixel as a separate entity, object-based methods use summary statistics of pixel groupings to produce a classified result (Aplin and Smith 2008). "Objects" are created by delineating the most internally homogenous groups of contiguous pixels that the classifier can identify. Idealized homogeneity of objects is based on compactness, shape, and colour (or spectral data in remote sensing applications), each with varying weights of importance as assigned by the user. Summary attributes are then calculated for each image object. These attributes can include statistical summaries of the pixel values which comprise the object (minimum, maximum, mean, standard deviation) or geometric attributes referring to the actual shape of the object (compactness, elongation, circularity, rectangularity).

The balance of the classification proceeds in a similar fashion to a traditional pixel-based supervised classification, where the user defines training sites whose underlying numerical values are used to define the spectral classes. Rather than include the values of each individual pixel, however, it is the summary statistic for the entire object that is used for the classification. This process is also an iterative method, and the user may modify the training sites after viewing the classified image to produce a more satisfactory result.

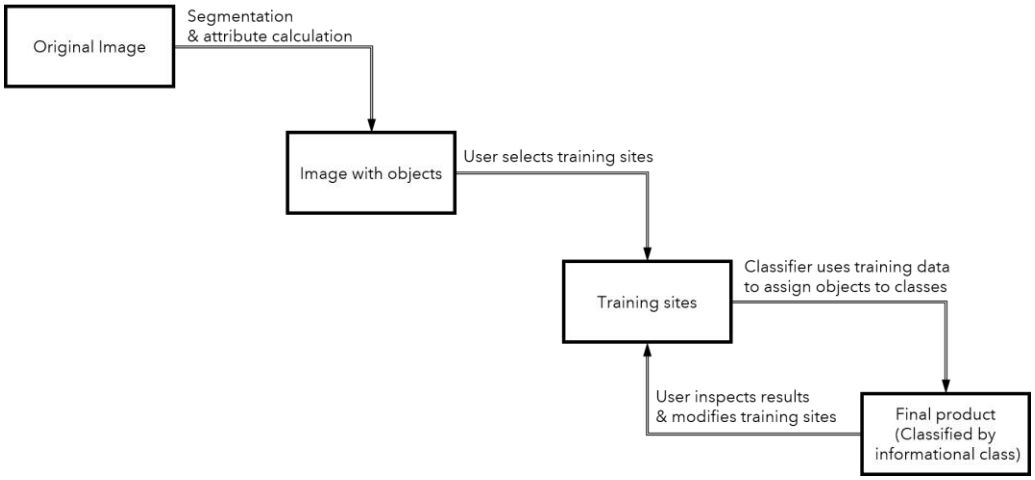

Figure 5. Simplified workflow of an object-based classification of multispectral remote sensor data.

2.3 Remote sensing background

2.3.1 What is a satellite image? Sensing the electromagnetic spectrum.

As described by Jensen (2005b), both the wave model and particle model of light are accepted conceptualizations of electromagnetic radiation (*EMR*) and are considered in remote sensing applications. According to the wave model, energy is comprised of electric and magnetic fluctuating fields at right angles to one another (Jensen 2005b). Types of EMR are described by their wavelength, which is the mean distance between peaks of these fluctuating signals, and typically the term *EM Spectrum* refers to wavelengths of energy between 0.001 nm (Gamma rays) to 100,000 km (extremely low frequency radio waves). The wavelengths of EMR that human eyes can detect, the *visual spectrum*, range from about 380 to 740 nm (Jensen 2005b).

Many optical multispectral sensors equipped to satellites are designed to detect several discrete ranges of wavelengths in the EM Spectrum, including wavelengths beyond the visual range of humans. The sensor systems used to collect imagery for this study all detect energy in the visual spectrum, via separate blue (~400–500 nm), green (~500–600 nm), and red (~600–700 nm) detectors, as well as energy in the near-infrared (NIR; ~700–1300 nm) and shortwave infrared (SWIR; ~1300–3000 nm) ranges. Each detector is designed to measure the amount of

radiation in a specific range of wavelengths, however the individual detectors are unable to discriminate between wavelengths inside of their designated range. As an example, a detector designed to collect a spectral range of 450–515 nm (or visible blue-green) can detect the total radiant flux over this entire range, but cannot differentiate between incoming energy at 450 nm from energy at 515 nm. It is also important to note, there can be some marginal detection just beyond the listed limits of the spectral range of the detector (*out-of-band response*; Mobley et al. 2016).

The sensors used to generate imagery for this study can also be classified as passive optical systems. Passive systems do not emit any source of energy themselves, but instead capture reflected EMR from some external source (i.e., illumination from the sun; Shippert 2004). There are a number of opportunities for interaction and degradation of the energy between the sun and the sensor—when it first encounters the top of the atmosphere, as it travels through the atmosphere, when it hits the ground, as it travels back through the atmosphere and back to space to finally interact with the sensor system (Figure 6).

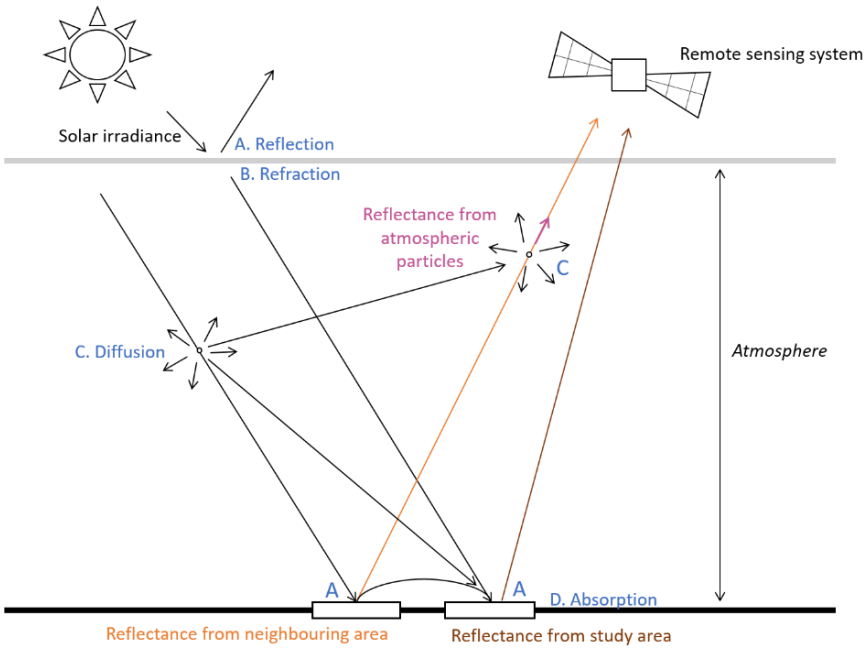

Figure 6. Simplified schematic of EMR interactions between the source and the sensor, and paths for EMR between the source and sensor. (Adapted from Jensen (2005b)*: Figure 6-24)*

Of particular importance are the interactions of EMR at the Earth's surface; when EMR interacts with ground-level features there are three possible interactions that could occur: reflection, absorption, or transmission of energy (Gilvear and Bryant 2016). How the surface of the feature interacts with different wavelengths of EMR depends on the characteristics of the interacting material. It is this surface interaction (in conjunction with atmospheric conditions) that determines the spectral response recorded by the sensors. Therefore, knowledge of how EMR interacts with different materials is the basis of geomorphological interpretation of remote sensing data.

Classification of land cover based on spectral response can be explained technically in terms of numbers, but it is essentially analogous to the interpretation we make of the world in front of us via our eyes; characteristic interactions of light with materials are interpreted by the brain as colours and visual textures that we use to distinguish features. Remote sensing can take this interpretation further by allowing us to "see" beyond the visual spectrum, to measure areas which are quite expansive or difficult to access, and to mathematically derive further information from a scene.

Let us return to the idea that any single sensor measures any detectable incoming energy over a defined range of wavelengths, and that a satellite often carries multiple detectors per sensor. The range of wavelengths measured by a single detector is referred to as a *band*, and the measurements received for an area on one band are represented by a single raster image that therefore shows only values measured in that range of wavelengths. A pixel value for a composite image can be conceptualized as a set of coordinates in multispectral space. In an image made up by three bands, any pixel can be thought of as having an *x, y, z* coordinate set, and the individual *x, y, z* values or any of their combinations can be used to describe the pixel and to assign it class membership. The values represented by pixels in satellite images are measures of remote sensing reflectance, as a scaled brightness value (BV). The possible range of BVs vary by the data storage component of the system (radiometric resolution, section 2.3.2).

Composite images allow the values of multiple arrays to be expressed simultaneously via the additive red, green, blue (RGB) colour model. The BV of each of three raster layers is used to inform the red, green, and blue component (or, *colour gun*) of the displayed colour for each. A common form of this type of symbology is the natural colour composite, where values from the red, green, and blue bands are assigned to the red, green, and blue colour guns, respectively (Figure 7).

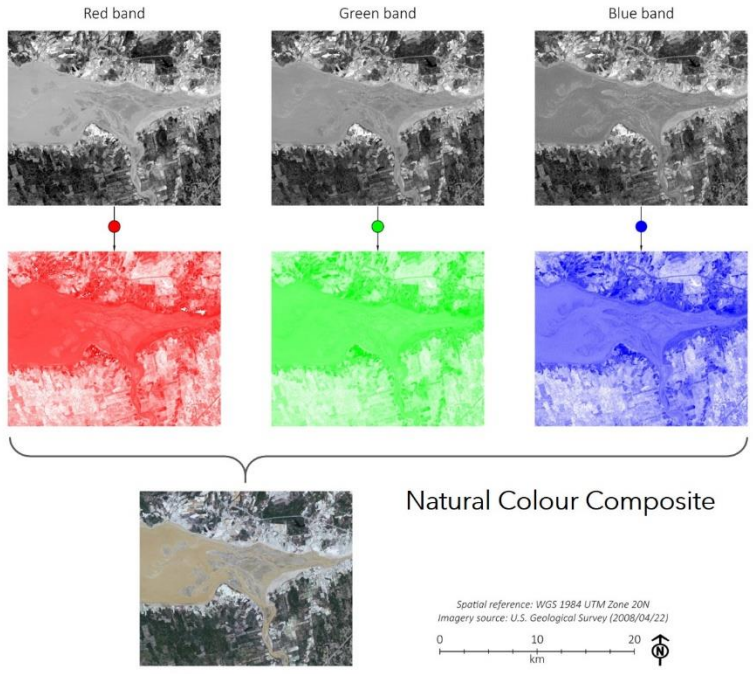

Figure 7. Natural (RGB) colour composite images are created by applying red, green, and blue colour scales to the red, green, and blue bands respectively, then combining them via additive colour theory.

In ideal circumstances, numerically defined spectral responses could be used to automatically pick out particular materials on the ground. However, the characteristics of the EMR is modified at a number of points in the path between the sun and the sensor—some interactions are more or less temporally stationary (certain land cover types, such as bedrock exposures) but many are variable through time and space (Gilvear and Bryant 2016). The endmember response (that is, the spectral response from an area of a single land cover type) in one image can be quite different for the same land cover in a different area, or recorded on a different day, due to differences in surface conditions (e.g., moisture content from recent

precipitation) or atmospheric conditions (Fraser et al. 1977). As such, a true "characteristic" spectral response is often difficult to define in terms of pure numbers. Inconsistent spectral response means that the spectral signature of a particular feature type, if we wish to use it to identify where this feature exists, often has to be re-defined for the conditions at the time of measurement. The repetitive analysis required to address many remote sensing and geomorphology questions informs this study and an important issue: if the analyst has to perform some series of tasks for every image, but has their choice of the actual method used, what is the least cost method that yields results exceeding the minimum acceptable standard?

2.3.2 Resolution

In a practical sense, resolution can be conceptualized as the frequency of sampling (Marceau 1999). Finer resolution gives increasing ability to differentiate smaller amounts of change, and the type of resolution is essentially the dimension in which this is captured. Satellite imagery can be described by four main types of resolution (see Table 2). While spatial resolution is the main focus of this project, it does not exist in isolation—all forms are qualities of the data which impact the result and should be noted.

Table 2. Characteristic resolution types of remote sensing data (Adapted from Jensen, 2005a).

Resolution type	Definition	Refers to
Spatial	Sampling frequency in terms of space; the lateral measurement interval	Pixel size; an image with 30m resolution have pixels that represent a space on the Earth that is 30m by 30m
Spectral	Division of the EMR spectrum for measurement; the range(s) of wavelength that are measured	Bands; a system can have multiple sensors that each measures a different range of wavelengths
Temporal	Sampling frequency in terms of time; the length of time between measurements	Revisit time; satellites in sun-synchronous orbit re-capture a scene at regular intervals at the same time of day
Radiometric	Increment of data storage	Bit depth; an image with 8-bit radiometric resolution stores BVs between 0 and 255, and an image with 12-bit resolution stores BVs between 0 and 4095

2.3.3 Details of satellite systems

A brief overview of the sensors from which imagery was retrieved is presented in Table 3. Each system measures visual and NIR wavelengths, with some having additional sensors to capture other parts of the EMR spectrum.

Table 3. Overview of system specifications of imagery sources.

Satellite system	Operation	Bands	Spatial resolution	Temporal resolution (at nadir)	Radiometric resolution
Landsat-5 Thematic Mapper (Kramer 2002)	Public; Operated by NASA & distributed by USGS	Visible Blue (450-520 nm) Visible green (520-600 nm) Visible red (630-690 nm) Near-infrared (760-900 nm) Shortwave infrared (1550-1750 nm) Shortwave infrared (2080-2350 nm) Additionally: Thermal (not included in analysis)	30m (Visible, NIR, SWIR) 120m (Thermal)	16 days	8-bit
Sentinel-2 Multispectral Instrument (Satellite Imaging Corp. 2017)	Public; European Copernicus Programme	Visible Blue (458-523 nm) Visible green (543-578 nm) Visible red (650-680 nm) Near-infrared (785-900 nm) Additionally; Coastal aerosol, red edge, water vapour, cirrus, Shortwave infrared (not available from U.S. Geological Survey)	10m (Visible & NIR)	5 days	12-bit
RapidEye (Satellite Imaging Corp. 2017a)	Private; operated and distributed by Planet Labs Inc.	Visible blue (440-510 nm) Visible green (520-590 nm) Visible red (630-685 nm) Near infrared (760-850 nm) Additionally: Red edge (not included in analysis)	5m	5.5 days	Collected at 12-bit; resampled to 16-bit
PlanetScope (Planet Labs Inc. 2019)	Private; operated and distributed by Planet Labs Inc.	Visible blue (440-510 nm) Visible green (520-590 nm) Visible red (630-685 nm) Near infrared (760-850 nm)	3m	1 day	Collected at 12-bit; resampled to 16-bit

2.4 Scale issues, part 2: Conceptualizing the relationship between scale of process and data

The value of a pixel at any location in remote sensing imagery is essentially an aggregated representation of the underlying land cover, and the pixel area is a homogenized unit. However, depending on the complexity of the area, this value may be more or less indicative of the actual land cover at any given spot. The relationship between scale and spatial complexity of the target phenomenon and the spatial resolution of the data manifests as a dominance by spectral endmembers, multi-feature pixels (mixels) or by multi-pixel objects (MPOs).

Spectral endmembers represent the spectral response of an area that contains a single land cover class (Jensen 2005d). Hypothetically, every BV in an image can be represented as a function of the proportion of endmember land cover classes contributing to the overall response. Therefore, a mixel is a single pixel which represents an area containing multiple feature types, with a value that reflects their proportional extent. Visually, mixels are often thought of as the fuzzy boundaries of ground features, making it difficult to find precise edges. The proportional occurrence of mixels depends considerably on spatial resolution; increasing sampling frequency decreases the space taken by mixels in an image (Hoyano and Komatsu 1988). It should be noted, however, that any pixel can be a mixel, depending on the scale of conceptualizing informational classes. This concept is illustrated in Figure 8; if we only wish to differentiate red from blue features, only pixel 1 is a mixel, while pixel 2 only contains one feature type. However, if we define three classes and wish to differentiate light from dark blue, pixel 2 is now also a mixel. In all cases, pixel 3 represents a spectral endmember, because the value is impacted by a single feature type (red).

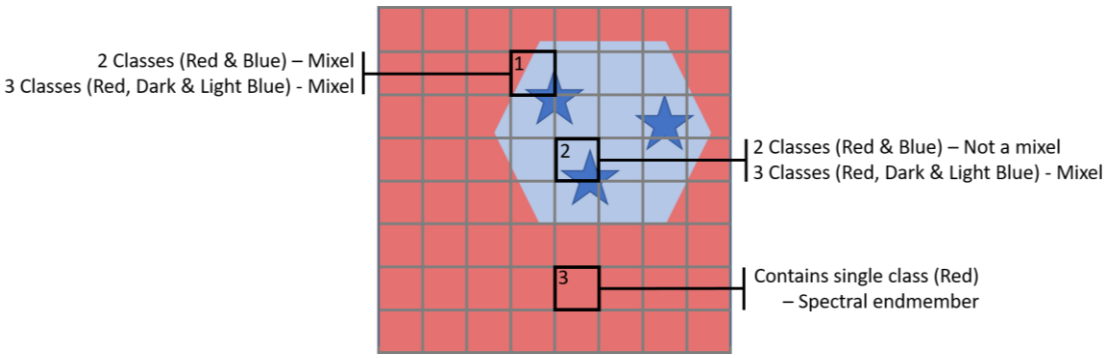

Figure 8. Simplified illustration of how scale of investigation and subsequent definition of informational classes influences the frequency of mixels.

In contrast to mixels, MPOs are homogenous features represented by multiple pixels (which thus have very similar values). It follows that at finer spatial resolutions, more pixels will be part of MPOs, and that more features will be represented by multiple pixels. Furthermore, the idea of an "object," and thus definition of an MPO in a scene, depends similarly on class definitions. This is illustrated in Figure 9; certain pixels may or may not be included in the central object depending on whether purple pixels are included or not. When creating objects for an object-based classification, the definition of boundaries is left to the classifying system and is based on parameters of idealized "likeness"—objects are created to be as internally homogenous and as different from their neighbours as possible (Blaschke et al. 2000).

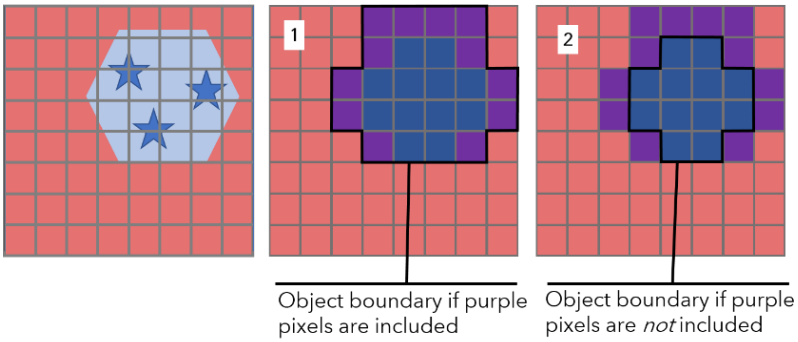

Figure 9. Simplified illustration of variation of object boundary definitions depending on decisions by the classifier relating to homogeneity.

The shift from mixel to MPO dominance in an image relates to the relative size of target features to the spatial resolution of the data. If the features are much smaller

than the area represented by the pixel, then it is likely that a single pixel contains multiple land cover types (i.e., the features would be contained within mixels). An "issue" with coarse spatial resolution, noted by Blaschke and colleagues (2014), is that the spectral response of potentially heterogeneous areas are aggregated to single values. Pixels representing larger areas can dilute or alter the spectral signature of the feature, possibly masking them, making their associated boundaries difficult to define, or exaggerating the area that they represent. Features which are much larger than the pixel size, however, would produce single-feature objects containing multiple pixels. In an ideal world, this result would mean an internally homogeneous cluster of pixels with a negligible boundary of mixels. Increasing the ratio of feature to pixel size leads to an overall decrease in mixels that partially contain the target features.

The visual relationship between resolvable detail and the image resolution is illustrated in Figure 10. Three images collected in the summer of 2010 were obtained; measured by the *Terra MODIS* (250m pixels), *Landsat-5* (30m pixels), and *RapidEye* (5m pixels) sensors. Images on the same horizontal line are shown at scales where their pixels are the same size on the page (and therefore, are shown at different scales relative to the features in situ). Images on the same vertical line show the same area, but their different spatial resolutions mean that different levels of detail are visible. The images shown at the same scale are strong examples of the impact of mixels on visualizing detail; the pairs of images are derived from measurements of the same area, but the consequence of the variable sampling frequencies is that less detail of the same features can be visualized in the coarser resolution images compared to their finer counterparts (compare Figure 10 B with D, and C with E).

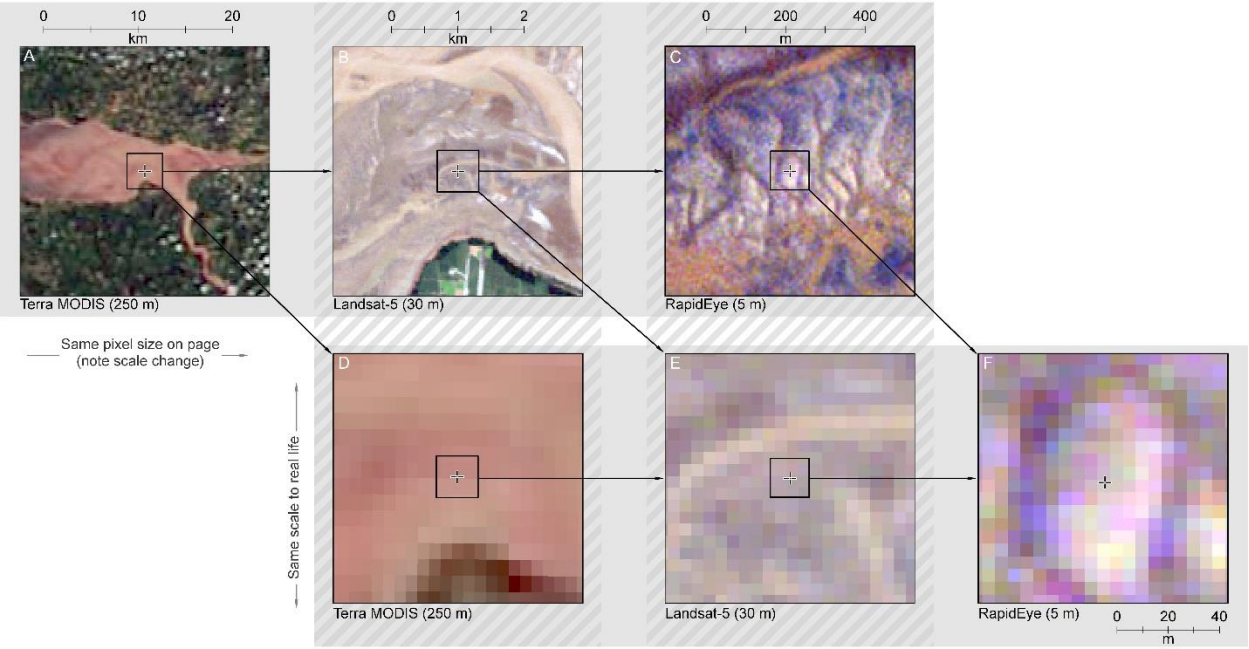

Figure 10. Selection of satellite images demonstrating the impact of variable image scale on the resolvable detail of features in Cobequid Bay (Terra MODIS imagery retrieved from NASA, 2010; Landsat-5 imagery from U.S. Geological Survey, 2010; RapidEye imagery from Planet Labs Inc., 2010).

2.5 Select related work

Bay of Fundy Tidal Barriers GIS Database Development (van Proosdij and Dobek 2005) and the *Minas Basin Estuary Profile* (COINAtlantic 2017)

Tidal barriers modify the flow regime and have an impact on sedimentation. While the impacts of large barriers are well known, the cumulative effects of the hundreds of smaller structures that are present around the Bay of Fundy are less well understood. This database includes detailed information of land-use surrounding the bay, and information on marshland development, but does not appear to include the intertidal bars.

The primary goal of the database, to assess the impacts of tidal barriers in the Upper Bay of Fundy to inform marshland restoration, aligns with this project's interest in assessing intertidal land cover classifications in the area. The apparently variable nature of the intertidal bars would suggest their importance to understanding sedimentation processes within the bay. Remote sensing provides a window into past

sedimentation regimes, which can aid in understanding current conditions and predicting future change to sensitive habitats.

A preliminary investigation into the spectral characteristics of inter-tidal estuarine sediments (Bryant et al. 1996) and *The influence of surface and interstitial moisture on the spectral characteristics of intertidal sediments: Implications for airborne image acquisition and processing* (Rainey et al. 2000)

These two papers focus on the Ribble Estuary, a macrotidal setting in the United Kingdom. Bryant and colleagues (1996) measured the spectral response of different clast sizes in the field and lab. It is stated that the spectral response of sediments is controlled by their organic matter and bulk mineral content. Sand samples exhibited high reflectance in the visual, NIR, and SWIR wavelengths in the field and lab. There was a negative relationship between increasing clay content and reflectance in these bands in the lab, which was not as easily seen in the field. This is attributed to the enhanced water retention after tide recession (which were therefore still wet when measured, compared to the dried lab samples) and more biological activity. The uncertainty in defining spectral response of sediments contributes to the challenges of remote sensing in estuarine settings; slow or variable drainage of bar sediments following tide recession, combined with the high suspended sediment content of the channel waters, create difficulty in teasing apart the two informational classes. In Cobequid Bay, the most confusion is expected to occur where there is poor drainage, which will likely record lower BVs than is characteristic for the overall feature, and where there is some local relief (such as ripple crests) which are more likely to record higher BVs.

Rainey and colleagues (2000) note further challenges of remote sensing for a phenomenon of this scale; the difficulty of mapping estuaries using satellite imagery, due to poor resolution on all counts, and of getting imagery that coincides both with good weather and good tides. They navigate this by using airborne imagery, but with new sources of imagery available since the publication of their paper, the question

can be raised again as to *how* limiting spatial resolution is to investigation of geomorphological problems at this scale.

Remote sensing and the measurement of geographical entities in a forested environment, part 1: The scale and spatial aggregation problem (Marceau et al. 1994)

Marceau and colleagues (1994) provide a framework for thinking about scale issues and remote sensing, especially related to the Modifiable Areal Unit Problem (MAUP; the sensitivity of analysis to the unit of data aggregation). In their study, a remotely sensed forest scene was systematically up-scaled to investigate relationships between MAUP and the ability to classify feature types. They conclude that the analysis of an image is inseparable from the sampling scheme (the systematic but arbitrary grid of the digital image). Indeed, any spatial phenomenon cannot be separated from its sampling scheme, because modifying the unit of analysis affects the framework of the investigation as well as any derived interpretation. Their results suggest that the sensitivity to MAUP can be tested by starting with a high spatial resolution image of a scene, and aggregating to coarser units of analysis to assess the impact on ability to detect spatial patterns. This work parallels their assertion through the use of progressively coarser spatial resolution from various sources, rather than resampling the original image.

Chapter 3. Methods

3.1 Image selection and preparation

3.1.1 Image acquisition

There are several variables to consider when acquiring satellite imagery. For this research, satellite images of the study area were selected on the basis of the following criteria:

1. Have less than 10% cloud cover within the study area. Clouds act as reflectors, and can block the spectral response from the ground surface (Astafurov et al. 2012). For the purpose of this investigation, clouds are nuisances because they reduce the area for analysis and can confuse the classifying algorithm.

2. Have been recorded between April and October, to avoid potential ice or snow cover.

3. Have been recorded when water level was less than approximately half the tidal range (i.e., within 3 hours of low tide) to maximize visibility of the bar surfaces and capture an image that is most representative of the actual bar–scour channel pattern that would be obscured by the flood tide.

The first two criteria took precedence and were met by all imagery included in the analysis. The third criterion could not always be confirmed (due to gaps in tidal record; see Appendix A.1) or met (due to lack of otherwise clear imagery; see Appendix A.5). The types of satellite imagery acquired are summarized in Table 4.

Table 4. Sources of imagery used for each classification of features in Cobequid Bay (2008-2019).

Satellite	Source	Spatial resolution	Repetitions	Bands used
Landsat 5	USGS	30 m	2	Visible, NIR, SWIR
Sentinel-2	USGS	10 m	3	Visible, NIR
RapidEye	Planet Labs Inc.	5 m	3	Visible, NIR
PlanetScope	Planet Labs Inc.	3 m	1	Visible, NIR

3.1.2 Pre-classification processing ("Cluster busting")

An early issue encountered was difficulty in differentiating water from sedimentary features when the whole image was considered for classification. The source of this issue was interpreted as a low spectral contrast of the water and bar classes, both compared to the other basin feature and to features on land. That is to say that the spectral difference between bar and water was less than the difference between, for example, water and open vegetation (one basin class compared to one onshore class), or between open vegetation and impervious surfaces (two onshore classes). As a result, classifications run on the image as a whole classified the entire basin as a single feature type and spent the other classes (in the example of unsupervised, where the system looks for a predetermined number of clusters) by splitting out details on the land. Because onshore land cover was not the target of this investigation, and to maximize the relative difference between feature types within the basin, the basin area was extracted and classified independently of the surroundings. This technique is known as *cluster busting*, used to break an assigned class down when it is known to contain multiple land cover types (Aksoy et al. 2013).

3.2 Classification

3.2.1 Unsupervised pixel-based classification

As discussed previously (see section 2.3.2), an unsupervised pixel-based classification assigns a categorical class to each pixel in the image, grouping based on some measure of spectral similarity. For each classification session, input channels (the bands, or single-sensor raster layers) are selected to be used for creating and assigning pixels to spectral groups.

Unsupervised classification was performed using the K-Means algorithm, with Null classes not allowed (that is, all areas must be assigned to some class). This algorithm iteratively computes centre of density of points in multispectral space until it identifies a predetermined number of point cluster centers (Hastie et al. 2009b). For each unsupervised classification, a maximum of 16 centers were identified after 64 iterations. The classifier then assigned pixels to classes as a function of the minimum

distance to a cluster center. The resulting spectral classes were aggregated by the user to two informational classes, sediment bar or water (Table 1).

It is noted that in most cases fewer than 16 clusters were identified by the initial classification, and that the number of target classes is actually 2 (+1 for areas outside the basin). However, minimizing the maximum number of centers resulted in poorer results than using too many. To avoid missing some of the more subtle spectral differences between informational classes, it seems to be a reasonable practice to overestimate the number of clusters in the initial run; the system will only return as many as it can find, and it is easier to aggregate several components of the same informational class than to bust clusters.

3.2.2 Supervised pixel-based classification

As described in section 2.3.3, the supervised classification operates with a reversed procedure to the unsupervised classification, where the user identifies training sites for each informational class, and the classifier uses those data to assign the remaining areas. For the supervised classifications, the classifier was trained on two informational classes, sediment bar and water (Table 1). Training sites were selected throughout the image to generate an approximately representative sample of the within-class spectral variability. Locations that would be used for the accuracy assessment (coinciding with an assessment point) were excluded from training.

Supervised classification was performed using the Maximum Likelihood algorithm, with Null classes not allowed. This algorithm uses the principles of probability related to Gaussian distribution to determine class membership, based on the z-score of a pixel in the context of the distribution of the training data for each of the classes (Hastie et al. 2009c).

After inspecting the results of the classification, there was the option to edit training sites. Where deemed necessary, training sites were modified and the classification was executed a second time. This process was repeated with modified

training sites until obvious areas of confusion were corrected, or until there was little return in quality of the classification result.

3.2.3 Object-based identification

Object-based classification uses computed summary values of classifier-delineated MPOs to produce the classification, instead of using the individual pixel values (as discussed in section 2.3.4). To perform the object-based analyses, the segmentation step was first applied to create the pixel clusters used for classification. Equal weight was applied to the compactness, shape, and colour parameters with regards to internal homogeneity of the objects. The size parameter (sometimes called the scale parameter) was varied depending on the spatial resolution of the source imagery, to maintain a reasonably constant "degree" of segmentation. Following segmentation, summary statistics (mean and standard deviation) for each object were computed to be used as the basis of the classification.

Objects were selected to produce the training data for the two informational classes (Table 1), avoiding locations coinciding with assessment points, and the classifier then assigned the rest of the objects to classes. Training sites could be modified after inspecting the result, reiterating until a satisfactory classification was produced.

3.3 Accuracy assessment

To assess the algorithm's classification, 200 random points were generated within the study area and visually classified by the user. Seeing that the entire classified study area was not being compared for each image, but just the classification at these discrete points, the same locations were used for every image to maintain comparability between assessments. Two statistics were reported for each classification: the proportion of overall agreement, and Cohen's Kappa.

Proportion of agreement was defined as number of points where the user and classifier identified the same informational class, divided by the total number of points. The Cohen's Kappa statistic is an indicator of improvement from a random

assignment, asking the question: knowing how many points the raters (the user or classifier) each assigned points to one class or the other, how much better is the agreement than if points were randomly assigned to classes in the same proportions (Cohen 1960)? As a proportion of agreement, a κ value of 0 indicates that the agreement of classification that is no better than random, and a κ value of 1 is a perfect agreement between the user and classifier. This is computed using equation 1 (variables described in Table 5). The assumptions of Cohen's Kappa are described in Table 7.

$$\kappa = \frac{p_o - p_c}{1 - p_c} \qquad \textit{(Eq. 1)}$$

Table 5. Variables used in equation 1 to calculate Cohen's Kappa for each classification.

Variable	Meaning
P_o	Observed agreement
P_c	Chance agreement, calculated using equation 2 (variables described in Table 6)

$$p_c = \frac{U_b \times C_b}{n^2} + \frac{U_w \times C_w}{n^2} \qquad \textit{(Eq. 2)}$$

Table 6. Variables used in equation 2 to calculate the proportional chance of agreement.

Variable	Meaning
U_b	Count of points identified by the user as bar
C_b	Count of points identified by the classifier as bar
U_w	Count of points identified by the user as water
C_w	Count of points identified by the classifier as water
n	Total number of points

Table 7. Assumptions of Cohen's Kappa coefficient (modified from Lund Research Ltd. 2018)

	Assumption	Context
1	*The categories are nominal and mutually exclusive.*	"Water" and "Bar" classifications have no hierarchy, and any point must be assigned to one or the other (not both).
2	*The observations are paired.*	The same set of points were assessed by the user and the classifier, and the comparison was made between the two assignments at each point.
3	*The same number of categories are used by both raters.*	All classifications were aggregated to two classes (Water and Bar) and user assignments were made using the same definitions.
4	*The raters are independent.*	To not influence one or the other, training sites for supervised classifications were not assigned to the same locations used for accuracy assessment. The user identification of accuracy points was performed without looking at the classified result.
5	*The same two raters judged all points*.	A single user (the author) classified the assessment points.

Chapter 4. Results

4.1 Quantitative results

Two examples of classification results are shown in Figures 9 and 10. Full-size versions of classification results for all images are provided in Appendix A.

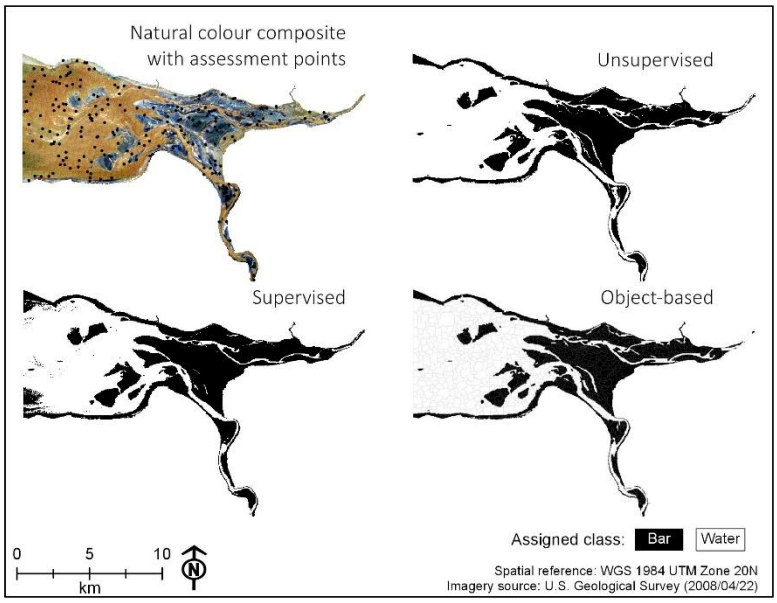

Figure 11. Classification results of Landsat 5 imagery (30m resolution; true colour composite; retrieved from USGS).

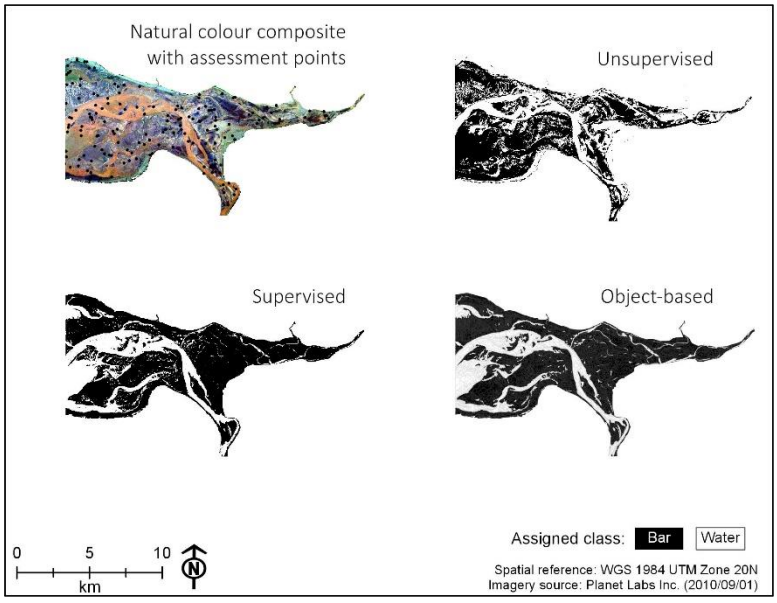

Figure 12. Classification results of RapidEye imagery (5m resolution, true colour composite, retrieved from Planet Labs Inc.)

The results of the accuracy assessments at each spatial resolution are reported in Table 8. The mean proportion of agreement and Cohen's Kappa are given for each data source, except for the PlanetScope imagery where only one image was used and therefore it is a raw value reported. It is important to note that the *n* of the reported mean values is very small (≤ 3). Given the small sample size, the mean values are potentially impacted by one-off outliers from the typical results of the data source. Of the reported mean values that could be considered "high" ($a > 0.8$, $\kappa > 0.8$) the range of raw values was within $a \pm 0.15$ and $\kappa \pm 0.10$ at most (results of pixel-based classifications of Landsat-5 imagery) and typically within $a \pm 0.04$ and $\kappa \pm 0.07$.

The unsupervised method shows an overall decreasing reliability with increasing spatial resolution. The proportion of agreement of the supervised method is consistent, although the Kappa statistic reveals decreasing reliability. The accuracy of the object-based methods remains consistent at all spatial resolutions.

Table 8. Results of accuracy assessments, reported as the mean or raw (*) proportion of agreement, a, and Cohen's Kappa, κ, for each data source.

Source	Spatial Resolution	*n*	Unsupervised (*a*, *κ*)	Supervised (*a*, *κ*)	Object-based (*a*, *κ*)
Landsat-5	30 m	2	0.81, 0.92	0.93, 0.85	0.97, 0.92
Sentinel-2	10 m	3	0.67, 0.37	0.93, 84	0.92, 0.82
RapidEye	5 m	3	0.76, 0.53	0.76, 0.53	0.96, 0.90
PlanetScope	3 m	1*	0.70, 0.32	0.98, 0.96	0.95, 0.90

4.2 Qualitative results: Unsupervised classification

There was an overall loss of quality of the unsupervised classification with increasing spatial resolution. At 30m, edges were maintained and the fine details of the delta channelization were captured, with some confusion on areas of the bar that have low overall BVs, perhaps appearing more wet than the surroundings due to finer sediments and poor drainage. At 10m, this method produced inconsistent results and was ineffective for two of the three images. At 5m, boundaries were identified but the result was otherwise poor. Confusion occurred on the water in areas of high

suspended sediment, on the bars in areas of poor drainage, and on highly reflective surfaces, At this resolution there were areas of dispersed single-pixel errors. At 3m, the result was very poor—the majority of the image was assigned to a single class, with only high-reflectance surfaces being classified separately.

4.3 Qualitative results: Supervised classification

Upon visual inspection, the supervised classification produced a similar quality of result at all spatial resolutions, notably with regard to edge preservation, but there were some differences. At 30m, smaller channels were not all captured, and there is some sensitivity to suspended sediment. At 10m, there was some single-pixel confusion around boundaries and wave crests. At 5m, the ability to capture the connectivity of the small channels varied by image. There were areas of dispersed single-pixel confusion, as well as confusion of highly reflective areas. At 3m, there were few areas of dispersed single-pixel errors around wave crests and on bars in areas of poor drainage.

4.4 Qualitative results: Object-based classification

While the quality of product was fairly consistent, the object formation and areas of confusion varied with spatial resolution. At 30m, the objects were blocky and, while conforming to boundaries, were otherwise independent of the underlying imagery. The bars were broadly captured, but some of the connectivity of the smaller channels was lost and there was some confusion in highly reflective areas. At 10m, objects were still somewhat blocky but more natural-looking than the coarser imagery. The size of the bars was slightly over-estimated; shape was generally preserved but the area encroached into the water. There was some loss of connectivity of the small channels and few instances of confusion on wave crests. At 5m, the objects were variable in shape and followed natural morphology seen in the imagery. There was still loss of channel connectivity, and confusion of highly reflective surfaces and areas of poor drainage on the bars. At 3m, the objects had natural-looking shapes, and the connectivity of smaller channels was well-preserved. There was some confusion around wave crests.

Chapter 5. Discussion

5.1 Discussion of results

To understand how spatial resolution of imagery impacts the reliability of image classification methods to identify estuarine sediment bars from satellite imagery, a simple comparison can be made between the Cohen's kappa statistics depending on pixel size and method of classification. The accuracy assessment results reveal three clusters of data: 1) low spatial resolution, high accuracy; 2) high spatial resolution, high accuracy; and 3) high spatial resolution, low accuracy (Figure 13).

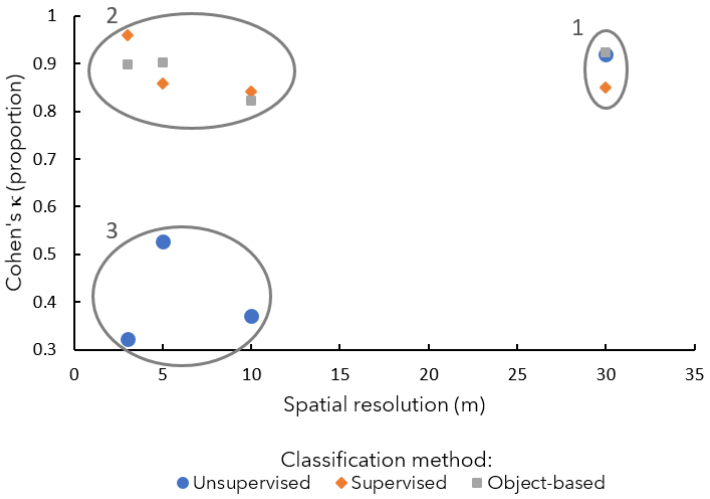

Figure 13. Mean Cohen's kappa statistics of classifications of the same spatial resolution and classification method plotted against spatial resolution of the source imagery.

If the proportion of overall agreement is plotted against spatial resolution (Figure 14), the cluster pattern is similar to that of the κ values, with the primary difference being that supervised classification of the 5m RapidEye imagery is included in the third group (higher spatial resolution imagery with low classification accuracy). Recall that the proportion of agreement is the probability that a given point was identified as the same informational class by the user and the classifier, while the Kappa statistic is the probability that the agreement was not obtained by random chance. Even moderate overall agreement with high confidence suggests a more

meaningful classification result than low values in both variables. As such, the dissonant point (supervised classification of RapidEye imagery) will be included in the second group for the sake of this discussion.

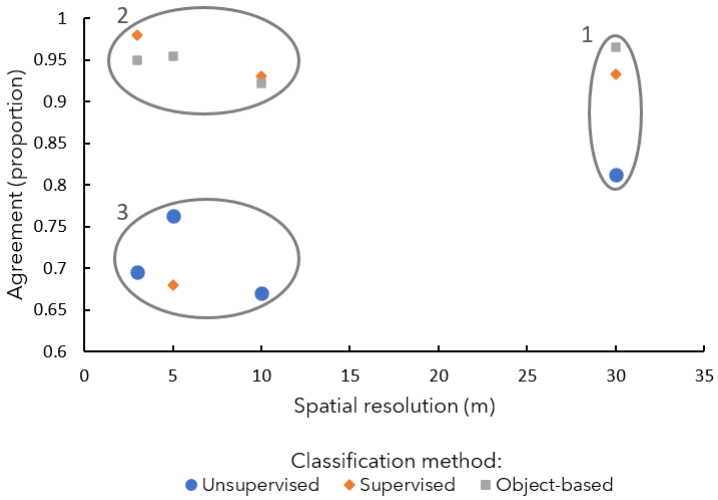

Figure 14. Mean proportion of agreement of classifications of the same spatial resolution and classification method plotted against spatial resolution of the source imagery.

First, the coarser spatial resolution (but higher spectral resolution) Landsat-5 imagery performed well (and consistently) under all three methods. It is intuitive to say that the "pre-smoothing" by larger sampling areas means that there is little advantage to additional aggregation by object segmentation. Note, however, that the points of disagreement fell primarily within the smaller bar channelization. While this smoothing is advantageous to the overall classification, mixels (especially around feature boundaries) make edges more difficult to identify, and classifications can suffer from information loss related to these fine-scale features.

The classification accuracy of high spatial resolution imagery was less consistent between methods compared to the coarser imagery. The finer imagery performed very well under OBIA-type classifications. Images with many MPOs seem to be best classified by grouping the objects and treating them as single entities. Again, this follows the logic of the rationale which led to the development of object-based classifications. Overall, the results of classifying the coarser imagery (by any

method) and the finer imagery (by object analysis) produce similar quantitative results. Indeed, the main difference is that the edges of features are smoother in the high spatial resolution imagery, by virtue of (1) smaller pixel size preserving more geometric fidelity and (2) a smaller mixel presence, as was expected *a priori*. The results of supervised classification of the finer spatial resolution imagery are also included in this group, due to the high accuracy scores achieved. However, the qualitative difference between classifications produced by pixel-based or object-based methods (discussed below) suggest that the pixel-based results are not quite as valid as their quantitative assessment suggests.

Finally, the lowest accuracy scores were obtained from the classifications of high spatial resolution by the unsupervised method. The classifier appears to be unable to find suitable spectral classes in the comparatively detailed high resolution imagery, which was expected—one of the issues that object-based classification methods were designed to address is the increased within-class heterogeneity of BVs that results from smaller sampling areas (Blaschke 2000). The excess of variability for the defined informational classes, and presence of "outliers" in many areas regardless of class, would cause difficulty for the classifier. I posit that the supervised pixel-based method did well because training sites can be selected to include that variability in the spectral definition of the classes, while on its own the classifier was unable to identify the appropriate clusters to match with the informational class definitions. Altering the unsupervised classifying algorithm threshold to consider data points that were nearer or further in multispectral space when identifying clusters did not improve the result.

From a qualitative perspective, there were changes in the quality and information value that resulted from each classification method related to changing spatial resolution. As was reflected in the accuracy assessments, the unsupervised method degraded in quality with decreasing pixel size. The supervised method, while

producing similar quantitative results at all levels, also became less satisfactory upon visual inspection.

Broadly speaking, most of the confusion occurred in areas that can be described as "water with high sediment content" or "sediment with high water content." While these are visually differentiable and should have distinct spectral response, increasing spatial resolution appears to increase the confusion of these areas, especially in the pixel-based methods. Finer spatial resolution (and finer radiometric resolution) has a greater ability to capture within-class variability. Including pixels with a greater range of BVs in a spectral class effectively broadens the definition for class assignment, and might be contributing to this confusion.

Increasing spatial resolution was also accompanied by increased single-pixel errors—Blaschke and colleagues' (2000) so-called "salt and pepper effect." This difficulty to identify single pixels may be attributed to the increasing ability to discriminate small, anomalously bright or dark areas that would have been washed out at coarser spatial resolutions. The *glint* phenomenon is a documented nuisance in imagery of bodies of water, caused by the reflection of light from the water surface at an angle equal to the sensor's viewing angle (Overstreet and Legleiter 2017). Corrections to remove glint contamination continue to be developed to address the issue, typically by modeling the sea-surface roughness (e.g., Ottaviani et al. 2008) or by using NIR reflectance as a proxy for amount of sun glint (e.g., Hedley et al. 2005). However, these methods are most well-established for open or optically-deep water settings, and less so for fluvial and estuarine settings (Overstreet and Legleiter 2017). Overall, glint is a more common problem in high spatial resolution imagery, and in lieu of mathematical corrections the effect can be minimized by the use of coarser-resolution imagery or by aggregating pixels to objects.

A final change with increasing spatial resolution which should be noted was the shape of objects created during the segmentation step of the object-based method. At coarser resolutions, the objects were blocky and fairly uniform across the

image, and decreasing pixel size produced more natural object shapes. While the uniformity of shapes did not appear to have a huge impact on the final classification results, it does imply that the shapes were created simply because the system had been instructed to do so, and that they did not represent particularly meaningful pixel groupings.

5.2 Scale issues, part 3: The Modifiable Areal Unit Problem and domains of scale

This was a long walk for the short statement that is: this study is an exemplar Modifiable Areal Unit Problem (MAUP). Both pixels and objects are areal units to which data about the area is aggregated, and changing the area represented affects the value of the pixel or object and thus the result of analysis. This concept is well established for geospatial studies, but perhaps less discussed from a remote sensing perspective.

The MAUP was described in depth by Openshaw and Taylor (1979; 1981), and relates to the sensitivity of spatial analysis to changing units of data aggregation. Study areas (and space) can be conceptualized either as open space where events occur, or an area over which there is continuous, albeit variable, occurrence of a phenomenon. There are a great number of ways a study area can be divided into non-overlapping units for analysis, and the choice of sampling scheme is often made by the researcher to meet some constraint of the study or the available data. These units of analysis are effectively arbitrary, and thus, modifiable. The characteristics of an areal unit are determined by aggregation of the underlying area. Therefore, changing the size or shape of the unit, in capturing different underlying data, will produce a different result.

Especially in complex areas (or with high spatial resolution imagery that captures a higher degree of complexity), pixels are isolated data points that in reality make up a larger spatial pattern, or contribute to the overall representation of a feature (Castilla and Hay 2008). Segmentation replaces pixels as the unit of spatial analysis with larger objects. Aggregation of data within a feature can be useful for the

treatment of high spatial resolution imagery where the individual pixel components of MPOs are not particularly connected to the spectral definition of an object, but as a whole produce a recognizable feature—what Blaschke (1995) refers to as "within-patch heterogeneity."

The concept of *domain of scale*, as described by Wheatley (2010), implies that the scale at which a phenomenon is investigated directly influences the outcome of analysis, and that certain relationships or interpretations are artifacts of the scale of observation. Sampling schemes and spatial units of analysis, whether they are pixels or objects, provide a constraining framework for viewing the study area. Interpretations of spatial patterns are dependent on the framework through which they are studied (Wiens 1989). In this context, larger pixels provide a similar functionality to objects created from small pixels. Their similar utility appears to be demonstrated by the ad-hoc segmentation of the coarser imagery, which does not have as great an impact on the quality of classification result as for the finer imagery. While at this scale of investigation the larger pixels did not lend themselves well to the creation of meaningful objects, the object-based method may well be applied to the same imagery to greater effect to identify phenomena with greater spatial extent.

5.3 Additional considerations for data selection

The role of the classifier is to supplement visual interpretation in a systematic, efficient, and cost-effective manner. The value of the tool is diminished if the cost of analysis outweighs the convenience of these methods. There can be cost associated with data acquisition—some imagery is freely available through public organizations (e.g., Landsat and Sentinel imagery acquired through the U.S. Geological Survey and the European Space Agency / Copernicus Program), while there are typically fees associated with the use of imagery acquired by private operations (e.g., Worldview imagery through Maxxar technologies).

The time required to process the imagery is also a necessary consideration. Supervised and object-based methods require the user to select training areas, often

a tedious and time-consuming task. Larger areas, high-resolution imagery, and large numbers of images take longer to process, independently of method. While this time investment may not be a concern when dealing with relatively few images, any additional steps or processing time can quickly add up for larger, more complex projects.

Depending on the period of study and rates of change of the target phenomenon, different satellite series may be more appropriate than others simply for reasons of comparability. For example, Landsat 4–8 (1982–present; NASA and USGS 2013) has maintained consistent spatial and spectral parameters for data continuity. Long term time series at the scale of this study would be very well suited to this series.

5.4 Limitations

5.4.1 User-introduced error (errors of commission)

The alternative to the system classifying land cover is the user manually picking out features, delineating each bar and channel. This would be comparatively time consuming, and subject to some arbitrary decision-making by the user in areas that are not easily distinguishable as one class or the other. The classifier, while also having to make certain decisions, at least has a known set of rules on which these decisions are based.

In using a classifying software, we are not asking the system to make the interpretation entirely on things that cannot be seen—unexpected patterns or phenomena may be revealed, but the *unexpected* versus the *unknown* is an important distinction to make. Informational classes can only be assigned in ways that are meaningful to the user, and thus not beyond the user's knowledge. The basis of the classification is still the user deciding which features they want to discriminate. The benefits of a classifying system are that it requires less user time, and that it is systematic. In the interest of rigorous science, the ideal tie-breaking decisions are structured, and not based on the best guess of the user. However, the user is a

meaningful baseline because their interpretation is the alternative to, and their opinion the deciding factor in, using a system-classified result. A classification of "reality" is only as good as our ability to interpret it, and if the classifier does not at least perform to human standards, then it is not worth using.

A possible source of error, therefore, lies in the examples (the training data) provided to the classifier by the user. False assignment by the user (errors of commission) can affect the definitions of spectral classes that are used by the classifier, and thus affect the result. I tried to minimize this type of error by selecting training sites that were within identifiable features, and staying away from boundaries where mixing of classes is most likely to occur. However, there are certain circumstances where errors of commission are unavoidable. One situation is in the selection of training sites for the object-based classification; the boundaries of the objects often, but do not always, line up with feature boundaries as would be drawn by the user. However, enough training sites to effectively create a statistical definition of a class must be selected and the user may have to include areas that do not entirely meet the definition of their assigned informational class.

5.4.2 Disagreement of other types of resolution

There was some disagreement between images related to the other forms of resolution, as described in Table 3. Because increasing resolution allows for finer details to be resolved and teased apart, they must be acknowledged as potential limitations of the comparability of classifications included in this study.

The coarsest imagery in terms of spatial resolution, from Landsat-5, had a finer spectral resolution due to the included SWIR band. The added dimension could have helped differentiate classes based on their values in multispectral space. Reflectance of SWIR can provide information about moisture content of the ground material (Yuan et al. 2019). However, the confusion of areas on the bar that appeared to have higher moisture content than their surroundings was observed in classifications at all spatial (and spectral) resolutions.

Increasing spatial resolution was accompanied by increasing radiometric resolution; Sentinel-2, RapidEye, and PlanetScope imagery are collected as 12-bit values, while Landsat-5 is 8-bit (Kramer 2002; 2017b; Planet Labs Inc. 2019). Greater bit depth allows the same scene to be represented by a wider range of possible BVs—the implication being that smaller differences in amount of reflected energy can be detected, potentially resulting in easier differentiation of classes. The impact of this difference could be reduced by converting the pixel values from scaled BVs to surface reflectance, using system conversion factors unique to each system; pixel values would then be expressed in common units and be more comparable to one another.

The inconsistencies between data sources outlined above raise a question about the methodology of this project—why not exclusively obtain high spatial resolution imagery and resample it to increasingly coarse spatial resolution, per the methodology of Marceau and colleagues (1994)? Resampling the same imagery would remove some of the limitations of this study, but may not be entirely representative of the results that can be obtained from the satellite imagery that is commonly used. In this study, imagery is acquired from different sources, in spite of their dissonance in other types of resolution, to assess the data that would most typically be applied to these types of geomorphology problems. While the approach taken here may be less neat a study of the pure relationship between pixel size and classification accuracy, it is an appropriate investigation of the tools (both methods and data) that are actually and readily available.

Chapter 6. Conclusion

To answer the question of how spatial resolution affects the results of image classification to identify intertidal bars in Cobequid Bay, satellite imagery spatial resolutions between 3m and 30m were each classified three ways (unsupervised and supervised traditional pixel-based methods, and an object-based method). The conclusions based on the results of these classifications can be summarized by two statements:

1. Pixel-based methods are reliable at coarser spatial resolutions, but have difficulty addressing the large amount and variability of data in images with fine resolution—unsupervised classifications specifically fall apart with decreasing pixel size, although unfortunately are the least time-consuming for the user.

2. The object-based method performs well over a range of spatial resolutions, but lends itself best to addressing the dominance of multi-pixel objects in the finer spatial resolution imagery.

These conclusions hold implications for change detection of surface features. Ideally, inputs to change detection analyses should have satisfactory boundary fidelity, and limited classification errors. Manual correction may be required, although to limit this, it appears that unsupervised classification of coarse imagery or object-based classification of fine imagery produce adequate results with limited "salt and pepper effect." A rate of change can only be estimated within a margin of uncertainty that is *at minimum* equal to the spatial resolution of the image, and there is therefore a compromise between ease of analysis and the spatial threshold of change detection. There is also a tradeoff between the wider margin of uncertainty that accompanies coarser imagery, and the apparent overestimation of sediment bar size by the finer imagery.

The problems related to scale are not unique to this setting—remote sensing of estuarine morphology in a microtidal or mesotidal environment would be subject

to similar considerations to scale of process and data. The framework of considering large pixels as aggregated objects in their own right, while understanding the limitations of pixel-based methods at fine spatial resolutions, can be applied to other uses of image classification methods on remote sensing data.

To return to the initial question of whether some critical threshold exists at which the ratio between scales of process and data become too great to reliably identify estuarine features, we see that any scale of data that is fine enough to capture spatial variability of the phenomenon will suffice with appropriate treatment. There is some amount of generalization required (to minimize the internal heterogeneity of features), which can be accomplished either at the data collection phase or during analyses.

References

Aksoy S, Bartalev S, Caetano M, Classification LC, Deb SK, Nathr RK, Fallis A., Ghorbani a., Pakravan M, Horning N, et al. 2013. Land cover classification methods, Version 1.0. J Plant Ecol. 3(1):863. doi:10.1017/CBO9781107415324.004.

Amos CL, Long BFN. 1980. The sedimentary character of the Minas Basin, Bay of Fundy. In: The coastline of Canada. Dartmout, NS: Atlantic Geoscience Centre, Geological Survey of Canada. p. 123–152. doi:10.4095/102221.

Aplin P, Smith G. 2008. Advances in object-based image classification. Int Arch Photogramm Remote Sens Spat Inf Sci. 37:725–728.

Astafurov VG, Rasskazchikova TM, Skorokhodov A V. 2012. Interpretation of data of cloud remote sensing from space in the visible range of the spectrum. Russ Phys J. 55(3):323–329. doi:10.1007/s11182-012-9815-4.

Benz UC. 2007. Defiens Imaging GmbH: Object-oriented classification and feature detection. IEEE Geosci Remote Sens Soc Newsl.(September):16–20.

Benz UC, Hofmann P, Willhauck G, Lingenfelder I, Heynen M. 2004. Multi-resolution, object-oriented fuzzy analysis of remote sensing data for GIS-ready information. ISPRS J Photogramm Remote Sens. 58(3–4):239–258. doi:10.1016/J.ISPRSJPRS.2003.10.002.

Blaschke, T., Lang, S., Lorup, E., Strobl, J., & Zeil P. 2000. Object-oriented image processing in an integrated GIS/remote sensing environment and perspectives for environmental applications. Environmental information for planning, politics and the public. 2(1995):555-570.

Blaschke T. 1995. Measurement of Structural Diversity with GIS - Not a Problem of Technology. In: JEC Joint European conference on Geographical Information. The Hague, Netherlands: IOS Press. p. 334–340.

Blaschke T. 2010. Object based image analysis for remote sensing. ISPRS J Photogramm Remote Sens. 65(1):2–16. doi:10.1016/J.ISPRSJPRS.2009.06.004.

Blaschke T, Burnett C, Pekkarinen A. 2004. Image Segmentation Methods for Object-based Analysis and Classification. In: de Jong SM, van der Meer FD, editors. Remote Sensing Image Analysis: Including the Spatial Domain. Springer. p. 211–236.

Blaschke T, Hay GJ, Kelly M, Lang S, Hofmann P, Addink E, Queiroz Feitosa R, van der Meer F, van der Werff H, van Coillie F, et al. 2014. Geographic Object-Based Image Analysis – Towards a new paradigm. ISPRS J Photogramm Remote Sens. 87:180–191. doi:10.1016/J.ISPRSJPRS.2013.09.014.

Bryant R, Tyler A, Gilvear D, McDonald P, Teasdale I, Brown J, Ferrier G. 1996. A preliminary investigation into the spectral characteristics of inter-tidal estuarine sediments. Int J Remote Sens. 17(2):405–412. doi:10.1080/01431169608949016.

Canadian Hydrographic Service (CHS). 2019. Burntcoat Head (#270): 2019 Tide Tables. Government of Canada, Dept. of Fisheries and Oceans. 4 p.

Cao C, Lam NS-N. 1997. Understanding the scale and resolution effects in remote sensing and GIS. In: Quattrochi DA, Goodchild MF, editors. Scale in Remote Sensing and GIS. p. 57–72.

Castilla G, Hay GJ. 2008. Image objects and geographic objects. In: Blaschke T, Lang S, Hay GJ, editors. Object-based image analysis: Spatial concepts for knowledge-driven remote sensing applications. Berlin: Springer. p. 93–112.

COINAtlantic. 2017. Bay of Fundy Estuary Profile: Minas Basin. Halifax, NS: The Coastal and Ocean Information Network Atlantic.

Crewe B, Brewster GR, Kolstee H, Gordon R. 2005. Sediment movement in the Salmon River Estuary , Truro , Nova Scotia. In: Percy JA, Evans AJ, Wells PG, Rolston SJ, editors. Proceedings of the 6th Bay of Fundy Workshop. Cornwallis, NS: Environment Canada - Atlantic Region. p. 123–125.

Fraser RS, Bahethi OP, Al-Abbas AH. 1977. The effect of the atmosphere on the classification of satellite observations to identify surface features. Remote Sens Environ. 6(3):229–249. doi:10.1016/0034-4257(77)90005-0.

Gilvear D, Bryant R. 2016. Analysis of remotely sensed data for fluvial geomorphology and river science. In: Kondolf GM, Piegay H, editors. Tools in fluvial geomorphology. John Wiley & Sons, Ltd. p. 103-132.

Hastie T, Tibshirani R, Friedman J. 2009a. Chapter 2. Overview of Supervised Learning. In: The Elements of Statistical Learning. Springer-Verlag. p. 9–42.

Hastie T, Tibshirani R, Friedman J. 2009b. Chapter 13. Prototypes and Nearest-Neighbors. In: The Elements of Statistical Learning. 2nd ed. Springer-Verlag. p. 459–484.

Hastie T, Tibshirani R, Friedman J. 2009c. Chapter 8. Model Inference and Averaging. In: The Elements of Statistical Learning. 2nd ed. Springer-Verlag. p. 261–294.

Hedley JD, Harborne AR, Mumby PJ. 2005. Technical note: Simple and robust removal of sun glint for mapping shallow-water benthos. Int J Remote Sens. 26(10):2107–2112. doi:10.1080/01431160500034086.

Hoyano A, Komatsu Y. 1988. Influence of Mixels on Land Cover Classification in Residential Areas Using Airborne MSS Data. ISPRS Arch. 27:399–408.

Jensen JR. 2005a. Chapter 1 - Remote Sensing and Digital Image Processing. In: Introductory Digital Image Processing: A Remote Sensing Perspective. 3rd ed. Pearson Prentice Hall. p. 1-34.

Jensen JR. 2005b. Chapter 6 - Electromagnetic Radiation Principles and Radiometric Correction. In: Introductory Digital Image Processing: A Remote Sensing Perspective. 3rd ed. Upper Saddle River, NJ: Pearson Prentice Hall. p. 175–226.

Jensen JR. 2005c. Chapter 9 - Thematic Information Extraction: Pattern Recognition. In: Introductory Digital Image Processing: A Remote Sensing Perspective. 3rd ed. Pearson Prentice Hall. p. 337–406.

Jensen JR. 2005d. Chapter 11 - Thematic Information Extraction: Hyperspectral Image Analysis. In: Introductory Digital Image Processing: A Remote Sensing Perspective. 3rd ed. Upper Saddle River, NJ: Pearson Prentice Hall. p. 431–466.

Kramer HJ. 2002. Landsat-4 and 5, In: Observation of the Earth and Its Environment: Survey of Missions and Sensors. Springer Verlag.

Lang S, Tiede D. 2007. Definiens Developer - Snapshot. Gis.bus - GeoBIT:34–37.

Liu JG, Mason PJ. 2016. Image classification. In: Image processing and GIS for remote sensing: Techniques and applications. 2nd ed. John Wiley & Sons, Ltd. p. 91–102.

Lund Research Ltd. 2018. Cohen's kappa using SPSS Statistics. Laerd Statistics. https://statistics.laerd.com/spss-tutorials/cohens-kappa-in-spss-statistics.php.

Marceau DJ. 1999. The scale issue in the social and natural sciences. Can J Remote Sens. 25(4):347–356. doi:10.1080/07038992.1999.10874734.

Marceau DJ, Gratton DJ, Fournier RA, Fortin JP. 1994. Remote sensing and the measurement of geographical entities in a forested environment. 2. The optimal spatial resolution. Remote Sens Environ. 49(2):105–117. doi:10.1016/0034-4257(94)90047-7.

Marceau DJ, Hay GJ. 1999. Remote sensing contributions to the scale issue. Can J Remote Sens. 25(4):357–366. doi:10.1080/07038992.1999.10874735.

McCarty HH, Hook JC, Knos DS. 1956. The measurement of association in industrial geography. State University of Iowa, Dept. of Geography. 143 p.

Meentemeyer V. 1989. Geographical perspectives of space, time, and scale. Landsc Ecol. 3(3):163–173. doi:10.1007/BF00131535.

Mobley CD, Werdell J, Franz B, Ahmad Z, Bailey S. 2016. Atmospheric correction for satellite ocean color radiometry. Greenbelt, MD: NASA, Goddard Space Flight Center. 86 p. doi: 10.13140/RG.2.2.23016.78081

NASA, USGS. 2013. LDCM Press Kit - Landsat Data Continuity Mission. 16 p.

Openshaw S, Taylor PJ. 1979. A million or so correlation coefficients: Three experiments on the Modifiable Areal Unit Problem. In: Wrigley N, editor. Statistical Applications in the Spatial Sciences. London: Pion. p. 127–144.

Openshaw S, Taylor PJ. 1981. The Modifiable Areal Unit Problem. In: Wrigley N, Bennett RJ, editors. Quantitative Geography; A British View. London: Routledge and Kegan Paul. p. 60–70.

Ottaviani M, Spurr R, Stamnes K, Li W, Su W, Wiscombe W. 2008. Improving the description of sunglint for accurate prediction of remotely sensed radiances. J Quant Spectrosc Radiat Transf. 109(14):2364–2375. doi:10.1016/J.JQSRT.2008.05.012.

Overstreet BT, Legleiter CJ. 2017. Removing sun glint from optical remote sensing images of shallow rivers. Earth Surf Process Landforms. 42(2):318–333. doi:10.1002/esp.4063.

Planet Labs Inc. 2019. Planet Imagery Product Specification. 97 p.

van Proosdij D, Dobek P. 2005. Bay of Fundy Tidal Barriers GIS Database Development. Halifax, NS: Saint Mary's University, Dept. of Geography. 38 p.

Rainey MP, Tyler AN, Bryant RG, Gilvear DJ, McDonald P. 2000. The influence of surface and interstitial moisture on the spectral characteristics of intertidal sediments: Implications for airborne image acquisition and processing. Int J Remote Sens. 21(16):3025–3038. doi:10.1080/01431160050144938.

RapidEye Satellite Sensors (5m). 2017a. Satell Imaging Corp. https://www.satimagingcorp.com/satellite-sensors/other-satellite-sensors/rapideye/.

Sentinel-2A Satellite Sensor (10 m). 2017b. Satell Imaging Corp. https://www.satimagingcorp.com/satellite-sensors/other-satellite-sensors/sentinel-2a/.

Shippert P. 2004. Spotlight on hyperspectral. Boulder, CO. www.geospatial_online.com/shippert.

Stea RR, Conley H, Brown Y. 1992. Surficial Geology of the Province of Nova Scotia - Map 92-3. Halifax, NS: Nova Scotia Department of Natural Resources, Mines and Energy Branch.

Wheatley M. 2010. Domains of scale in forest-landscape metrics: Implications for species-habitat modeling. Acta Oecologica. 36(2):259–267. doi:10.1016/J.ACTAO.2009.12.003.

Wiens JA. 1989. Spatial Scaling in Ecology. Funct Ecol. 3(4):385–397. doi:10.2307/2389612.

Yuan J, Wang X, Yan CX, Wang SR, Ju XP, Li Y. 2019. Soil moisture retrieval model for remote sensing using reflected hyperspectral information. Remote Sens. 11(3). doi:10.3390/rs11030366.

Appendix A: Satellite imagery and classification results

This appendix contains the satellite images and results of their classifications.

A.1 Landsat-5, April 22, 2008

Product Identifier: LT05_L1TP_008028_20080422_20161101_01_T1

Collection start time: 2008:113:14:50:05.5314400

Approximate tidal phase: *exact phase unknown*

Confusion matrices:

		Reference class								
		Unsupervised			Supervised			Object-based		
	Classes	Bar	Water	Total	Bar	Water	Total	Bar	Water	Total
Map class	Bar	84	7	91	86	5	91	84	1	85
	Water	2	107	109	0	109	109	2	113	115
	Total	86	114	200	86	114	200	86	114	200
	a; κ	0.96; 0.91			0.98; 0.95			0.99; 0.97		

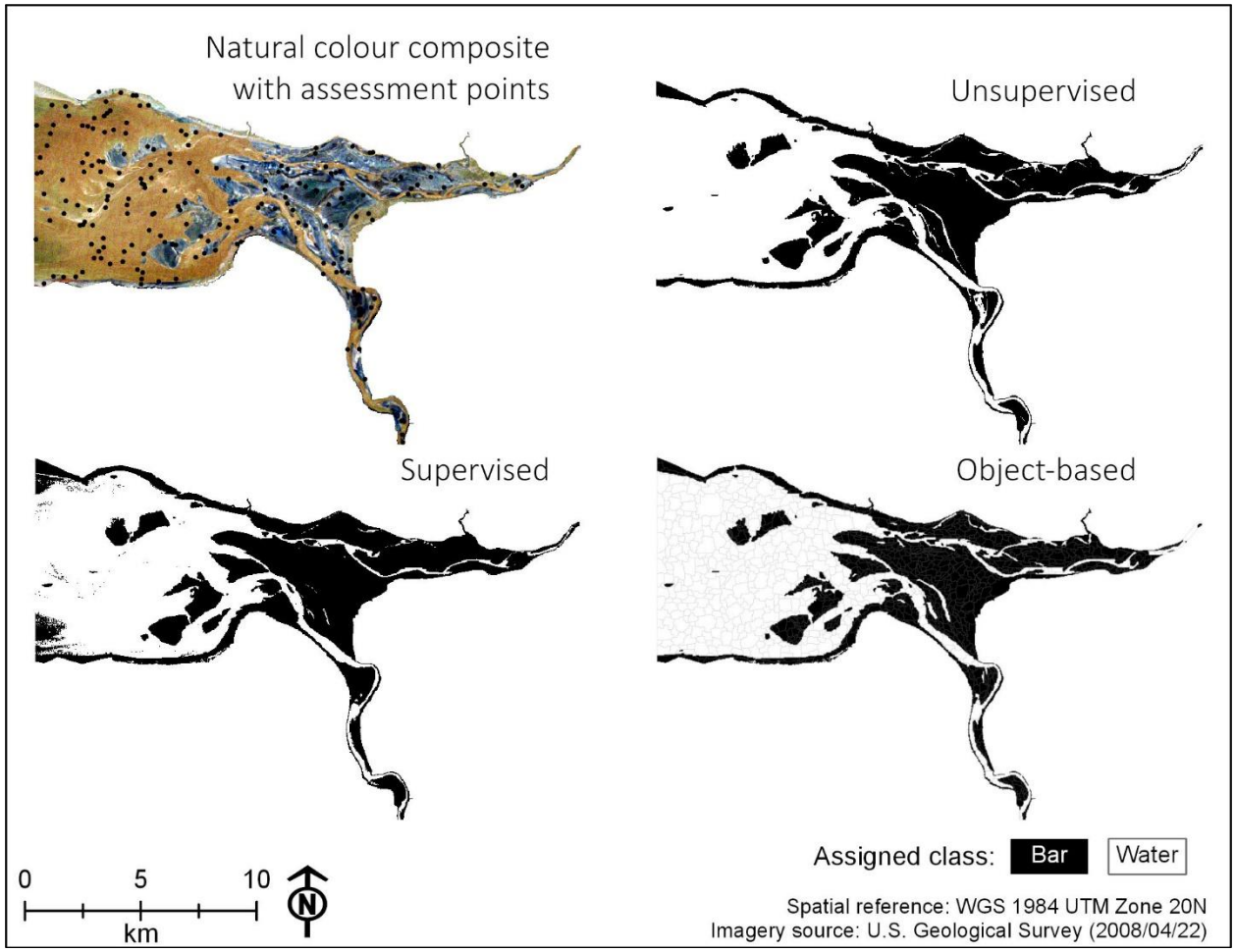

Classification results

A.2 Landsat-5, July 1, 2010

Product Identifier: LT05_L1TP_008028_20100701_20161014_01_T1

Collection start time: 2010:182:14:51:31.1128800

Approximate tidal phase: 2 hours following low tide

Confusion matrix

Reference class

Map class	Unsupervised			Supervised			Object-based		
Classes	Bar	Water	Total	Bar	Water	Total	Bar	Water	Total
Bar	**129**	15	144	**134**	4	138	**128**	3	131
Water	7	**49**	56	2	**60**	62	8	**61**	69
Total	136	64	**200**	136	64	**200**	136	64	**200**
a; κ	0.67; 0.93			0.89; 0.75			0.94; 0.88		

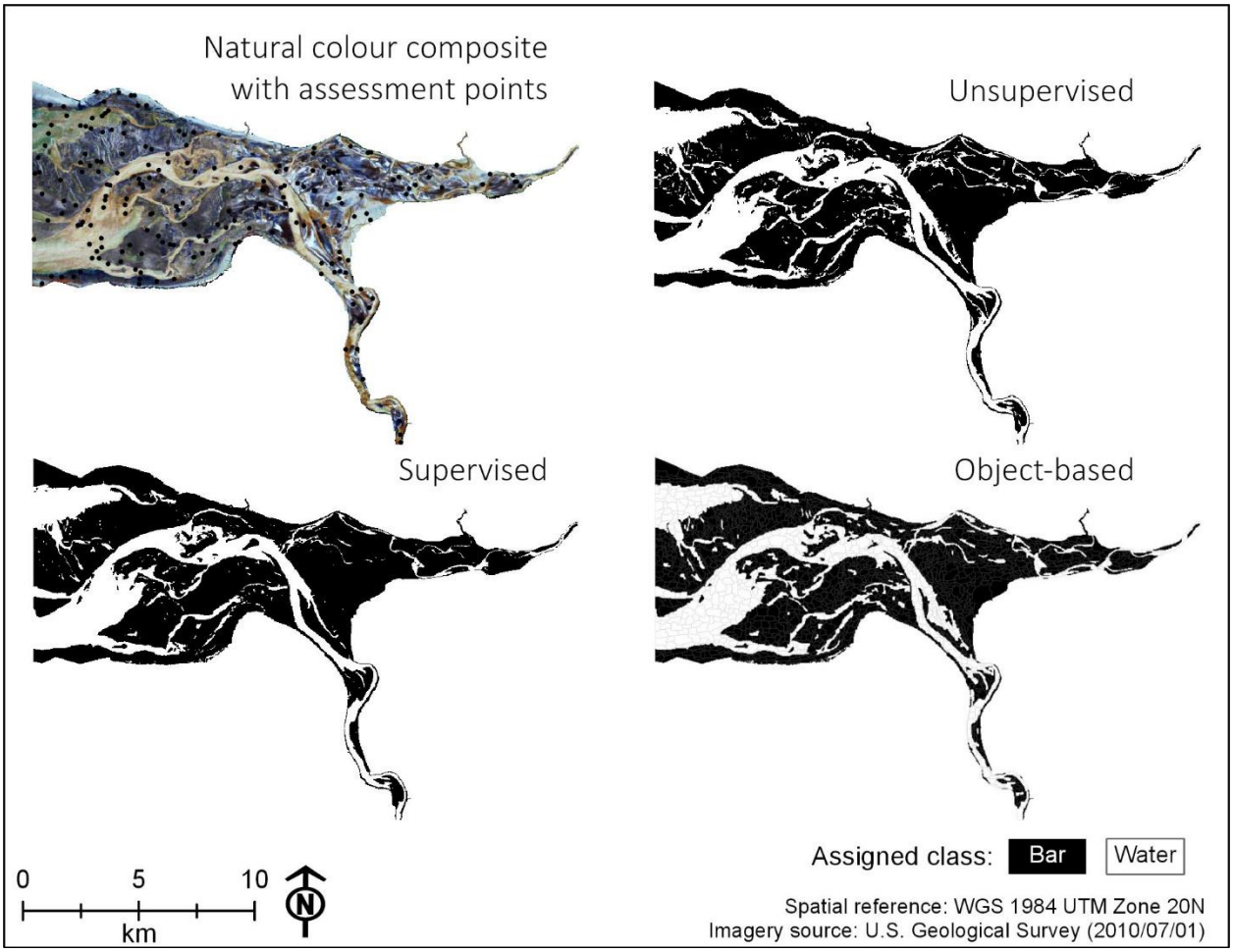

Classification results

A.3 Sentinel-2, May 9, 2016

Entity ID: S2A_OPER_MSI_L1C_TL_SGS__20160509T152240_20160509T203456_A004598_T20TMR_N02_02_01

Collection start time: 2016-05-09T15:16:43.461Z

Approximate tidal phase: 3.5 hours following low tide (2.5 hours prior to high tide)

Confusion matrix

		Reference class								
		Unsupervised			Supervised			Object-based		
	Classes	Bar	Water	Total	Bar	Water	Total	Bar	Water	Total
Map class	Bar	65	13	78	80	8	88	81	13	94
	Water	20	102	122	5	107	112	4	102	106
	Total	85	115	200	85	115	200	85	115	200
	a; κ	0.84; 0.66			0.94; 0.87			0.92; 0.83		

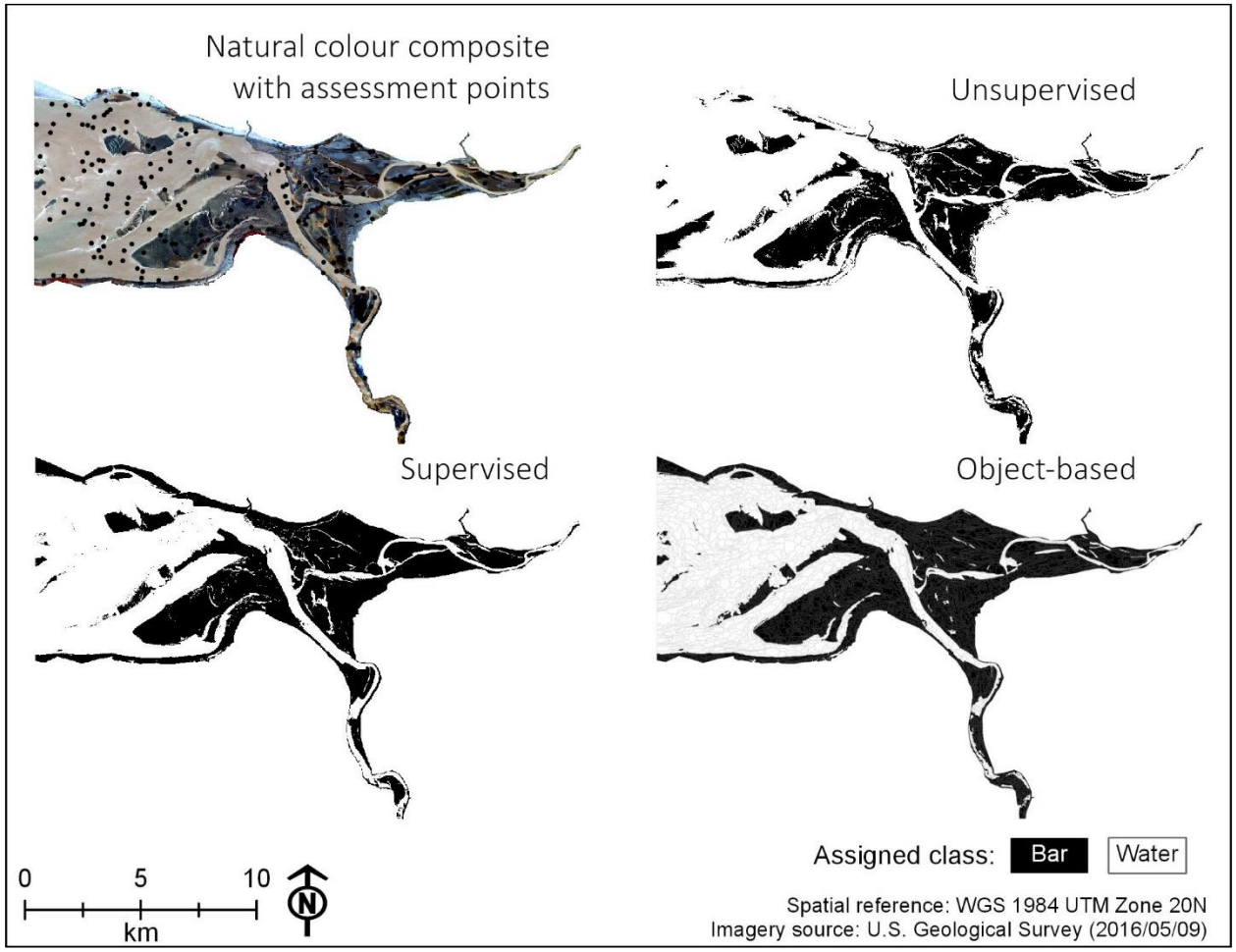

Classification results

A.4 Sentinel-2, May 4, 2017

Entity ID: L1C_T20TMR_A009746_20170504T151653

Collection start time: 2017-05-04T15:16:53.456Z

Approximate tidal phase: 1.5 hours prior to low tide

Confusion matrix

		Reference class								
		Unsupervised			Supervised			Object-based		
	Classes	Bar	Water	Total	Bar	Water	Total	Bar	Water	Total
Map class	Bar	**41**	67	108	**58**	14	72	**59**	14	73
	Water	23	**69**	92	6	**122**	128	5	**122**	127
	Total	64	136	**200**	64	136	**200**	64	136	**200**
	a; κ	0.55; 0.14			0.90; 0.78			0.91; 0.80		

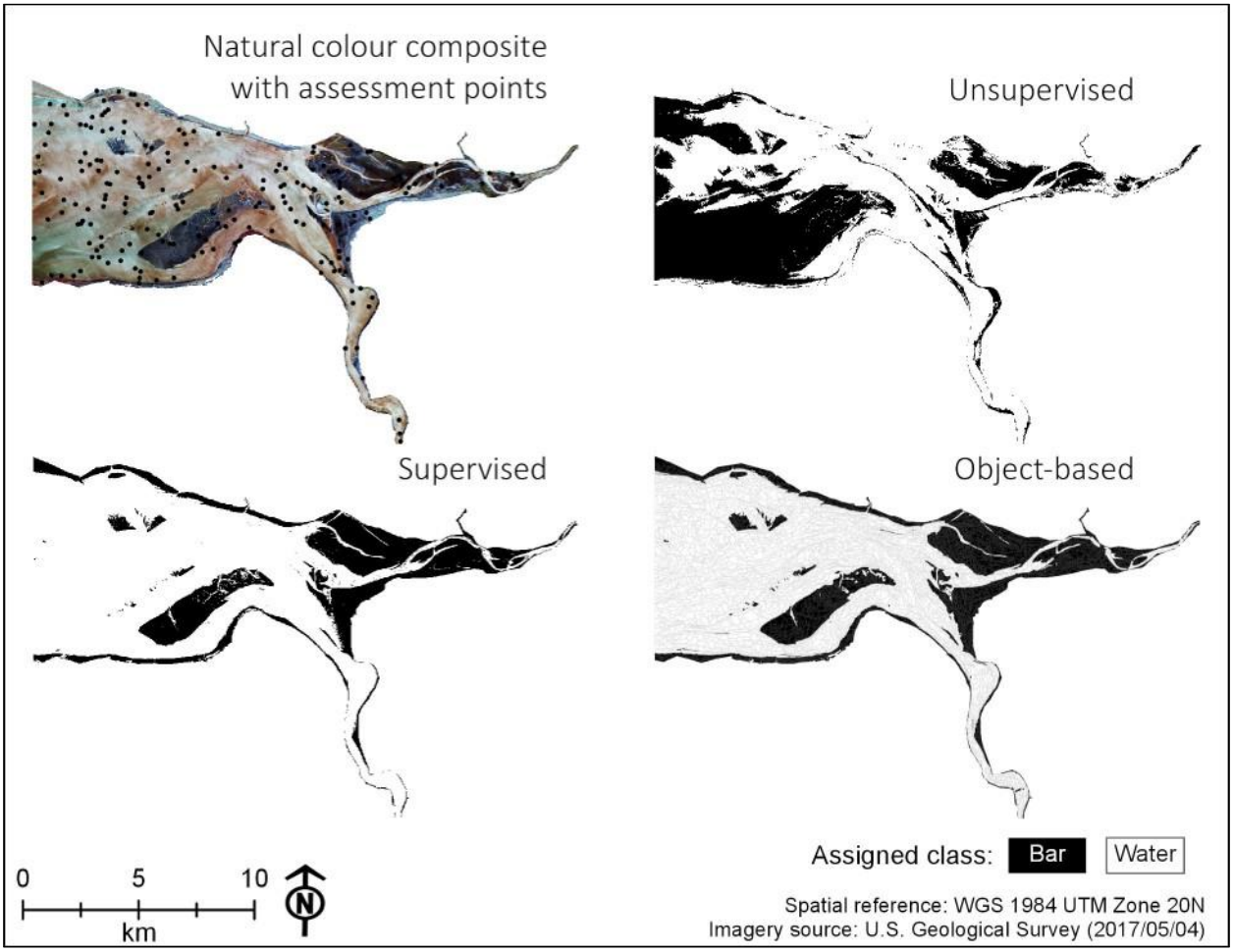

Classification results

A.5 Sentinel-2, August 2, 2019

Entity ID: L1C_T20TMR_A021472_20190802T151908

Collection start time: 2019-08-02T15:19:08.948Z

Approximate tidal phase: 4.5 hours following low tide (1.5 hours prior to high tide)

Confusion matrix

		Reference class								
		Unsupervised			Supervised			Object-based		
	Classes	Bar	Water	Total	Bar	Water	Total	Bar	Water	Total
Map class	Bar	44	73	117	41	4	45	38	3	41
	Water	1	82	83	4	151	155	7	152	159
	Total	45	155	200	45	155	200	45	155	200
	a; κ	0.63; 0.31			0.96; 0.87			0.95; 0.84		

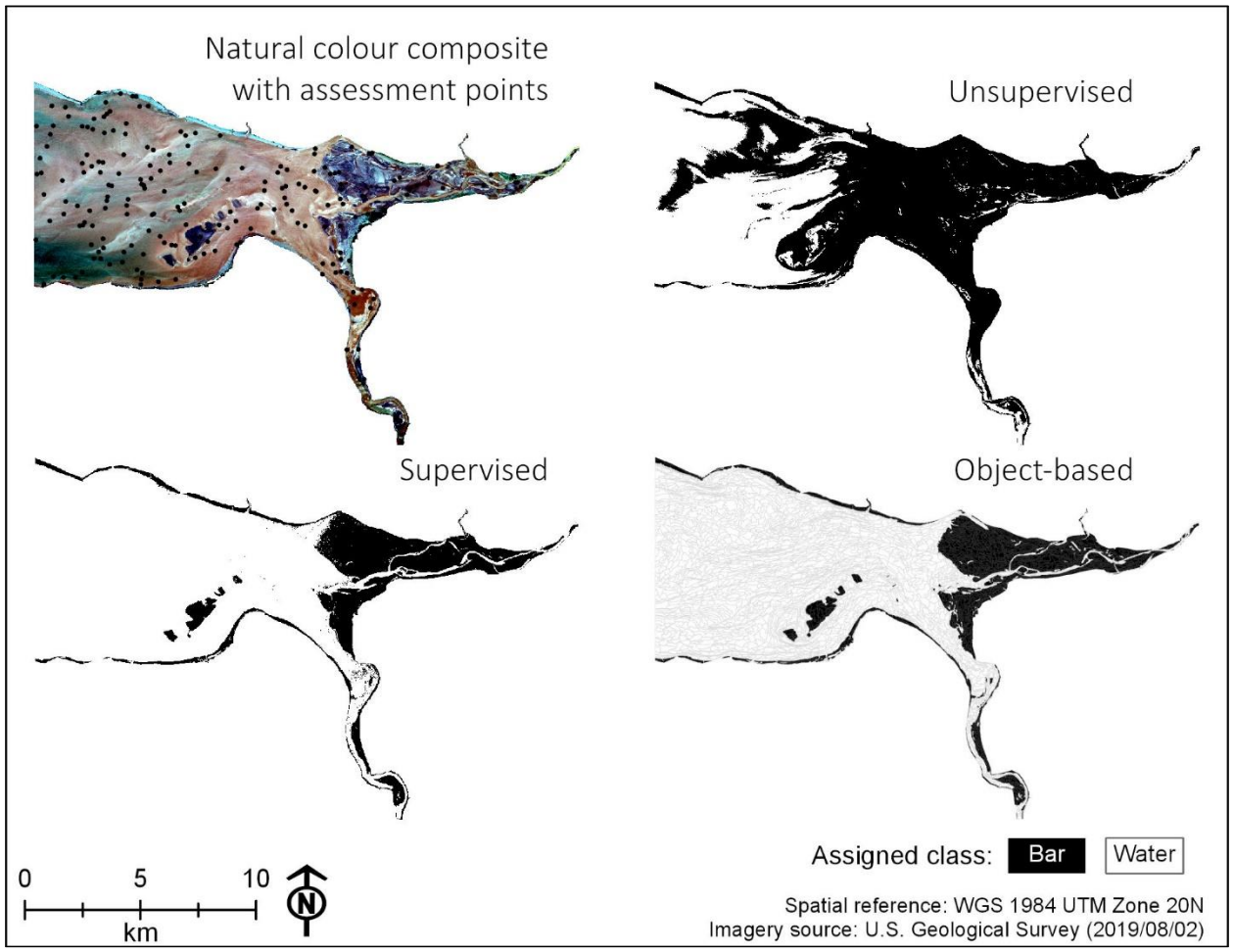

Classification results

A.6 RapidEye, September 1, 2010

Product Identifier: 20100901_160410_2060013_RapidEye-1

Collection time: 2010-09-01T16:04:10Z

Approximate tidal phase: 1.5 hours following low tide

Confusion matrix

Reference class

Map class	Classes	Unsupervised			Supervised			Object-based		
		Bar	Water	Total	Bar	Water	Total	Bar	Water	Total
	Bar	**96**	8	104	**58**	35	93	**97**	5	102
	Water	1	**49**	50	39	**22**	61	0	**52**	52
	Total	97	57	**154**	97	57	**154**	97	57	**154**
	a; κ	0.52; -0.02			0.15; 0.84			0.97; 0.93		

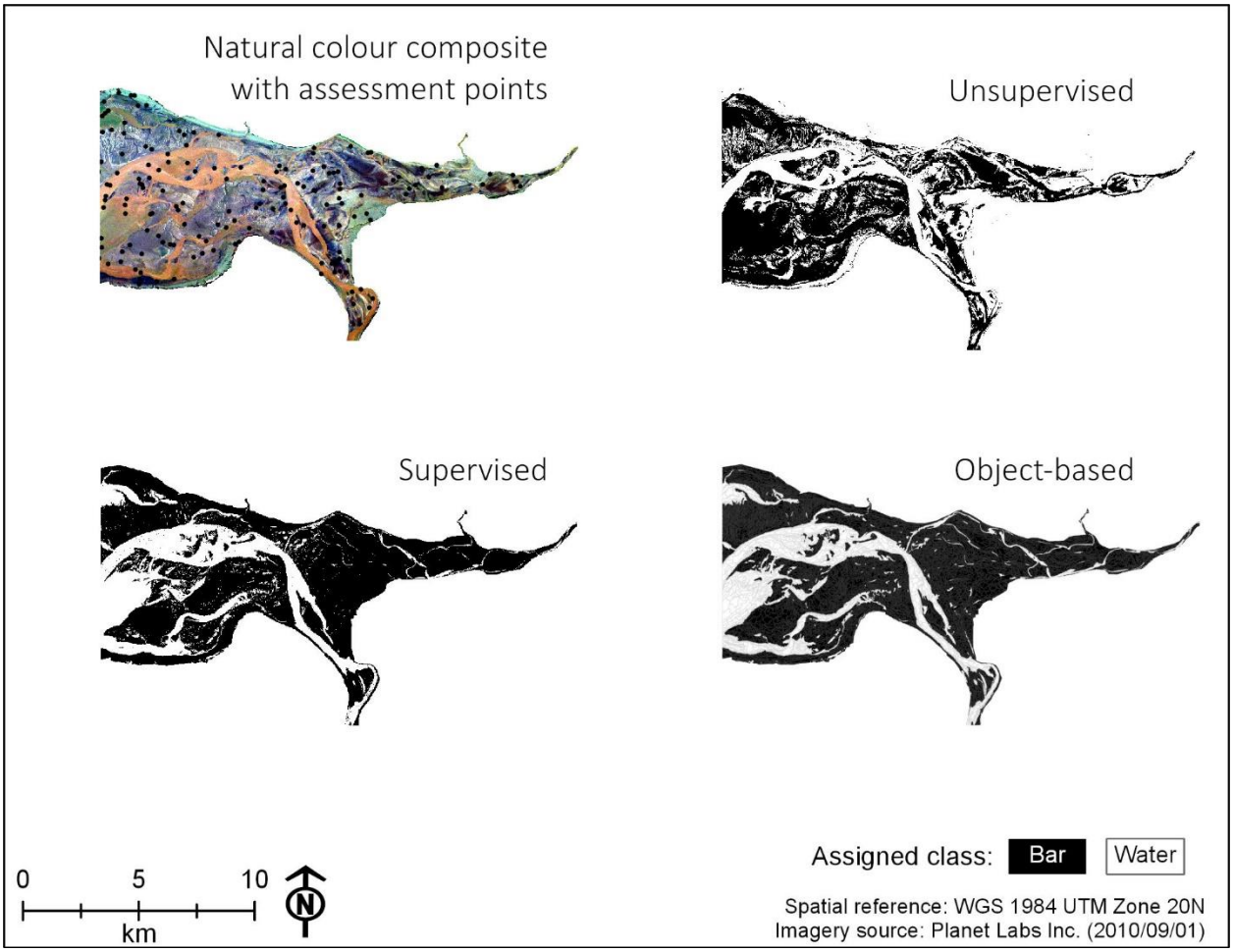

Classification results

A.7 RapidEye, July 15, 2013

Product ID: 20130715_RapidEye

Collection time: *exact time unknown; assumed to be approximately 16:00 due to sun-synchronous orbit of satellite*

Approximate tidal phase: *exact phase unknown; assumed 1.5 hours following low tide*

Confusion matrix

		Reference class								
		Unsupervised			Supervised			Object-based		
	Classes	Bar	Water	Total	Bar	Water	Total	Bar	Water	Total
Map class	Bar	105	2	107	131	8	139	134	12	146
	Water	31	62	93	5	56	61	2	52	54
	Total	136	64	200	136	64	200	136	64	200
	a; κ	0.84; 0.76			0.94; 0.85			0.93; 0.83		

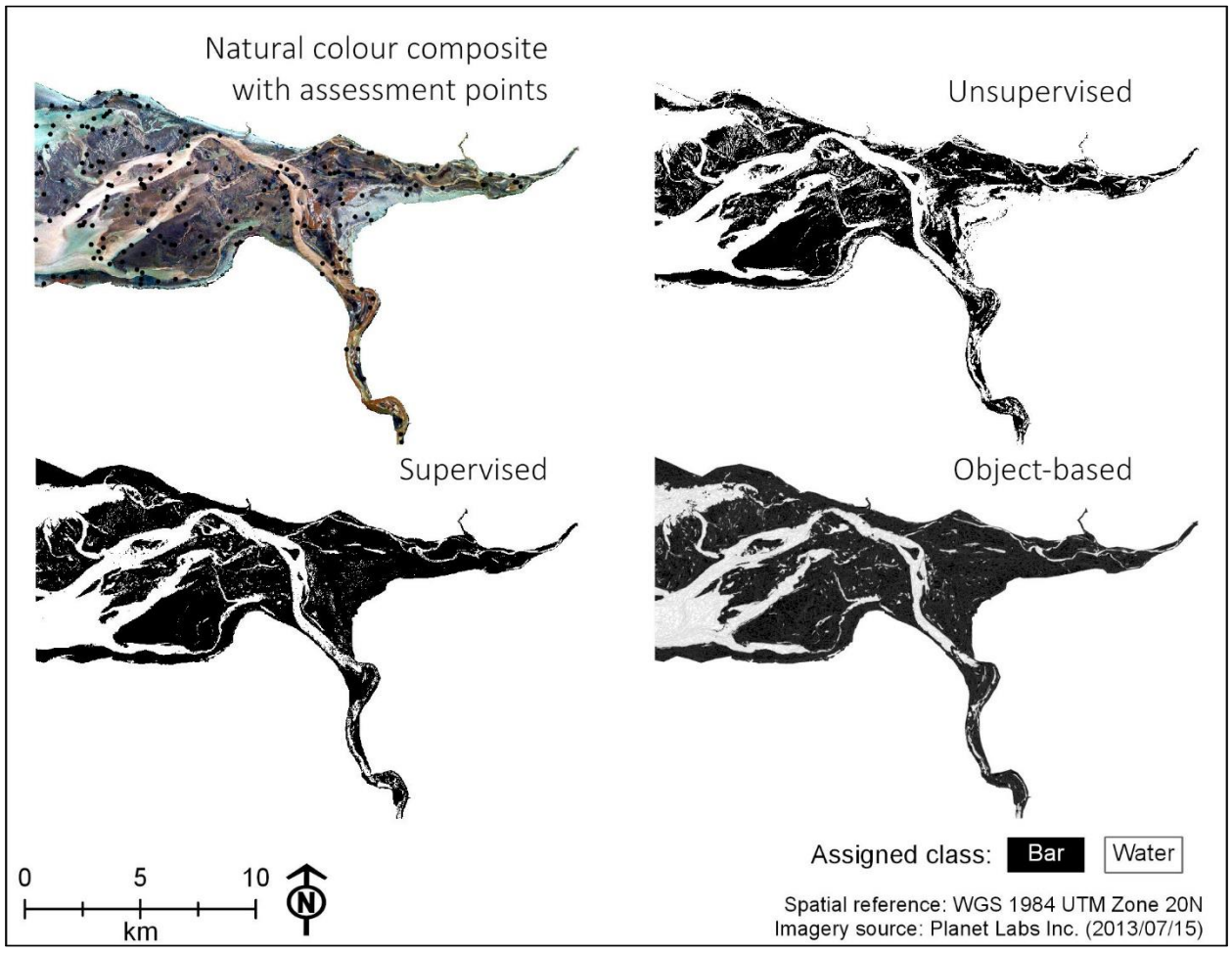

Classification results

A.8 RapidEye, September 19, 2019

Product ID: 20190919_145601_2060013_RapidEye-2

Collection time: *exact time unknown; assumed to be approximately 16:00 due to sun-synchronous orbit of satellite*

Approximate tidal phase: *exact phase unknown; assumed 3 hours following low tide*

Confusion matrix

		Reference class								
		Unsupervised			Supervised			Object-based		
	Classes	Bar	Water	Total	Bar	Water	Total	Bar	Water	Total
Map class	Bar	**106**	0	106	**110**	1	111	**112**	1	113
	Water	10	**38**	48	6	**37**	43	4	**37**	41
	Total	116	38	**154**	116	38	**154**	116	38	**154**
	a; κ	0.94; 0.84			0.95; 0.88			0.97; 0.95		

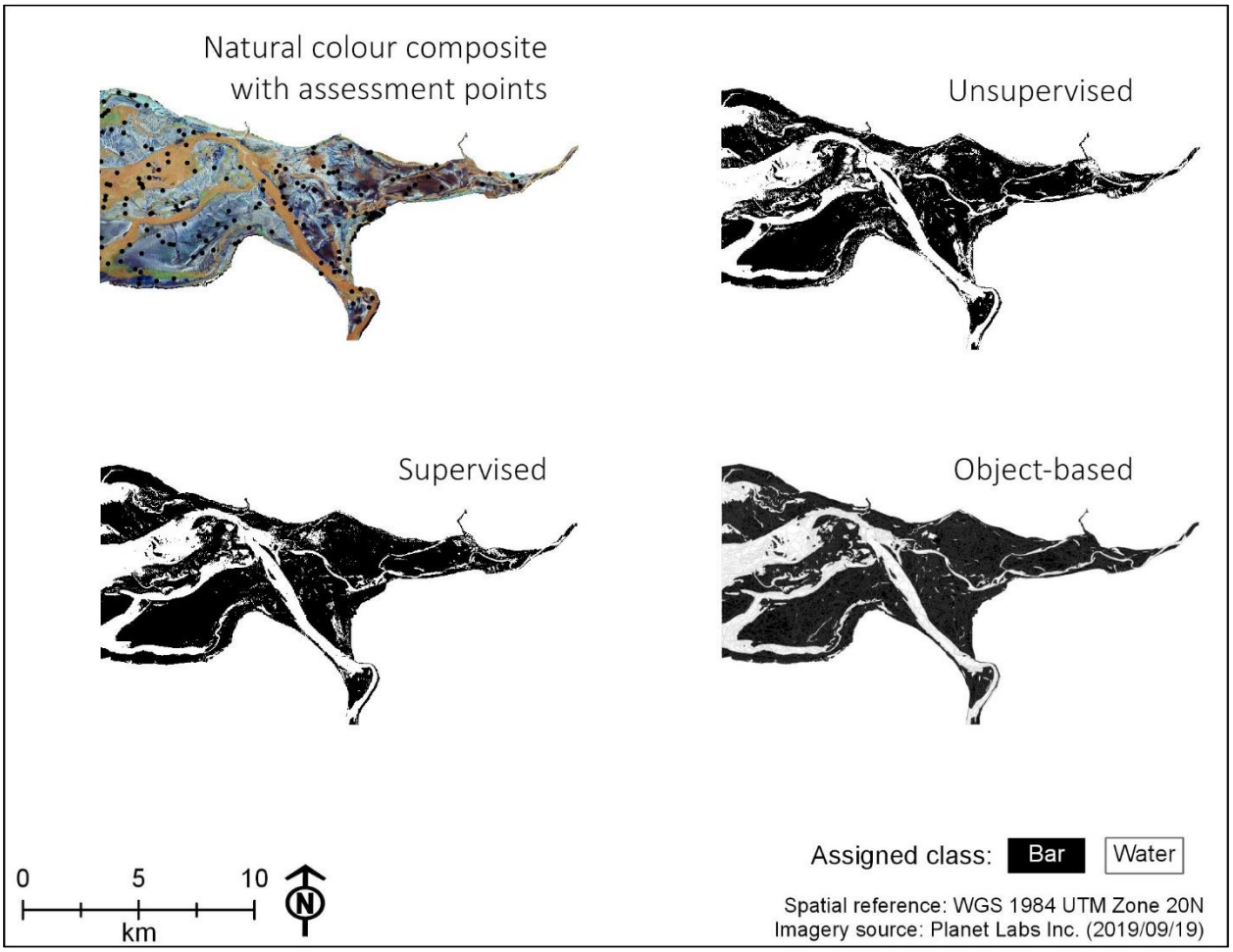

Classification results

A.9 PlanetScope, July 10, 2017

Product ID: Planet_20170710

Collection time: *unknown*

Approximate tidal phase: *exact phase unknown*

Confusion matrix

		Reference class								
		Unsupervised			Supervised			Object-based		
	Classes	Bar	Water	Total	Bar	Water	Total	Bar	Water	Total
Map class	Bar	**32**	3	35	**82**	2	84	**89**	3	92
	Water	58	**107**	165	8	**108**	116	1	**107**	108
	Total	90	110	**200**	90	110	**200**	90	110	**200**
	a; κ	0.70; 0.32			0.98; 0.96			0.95; 0.90		

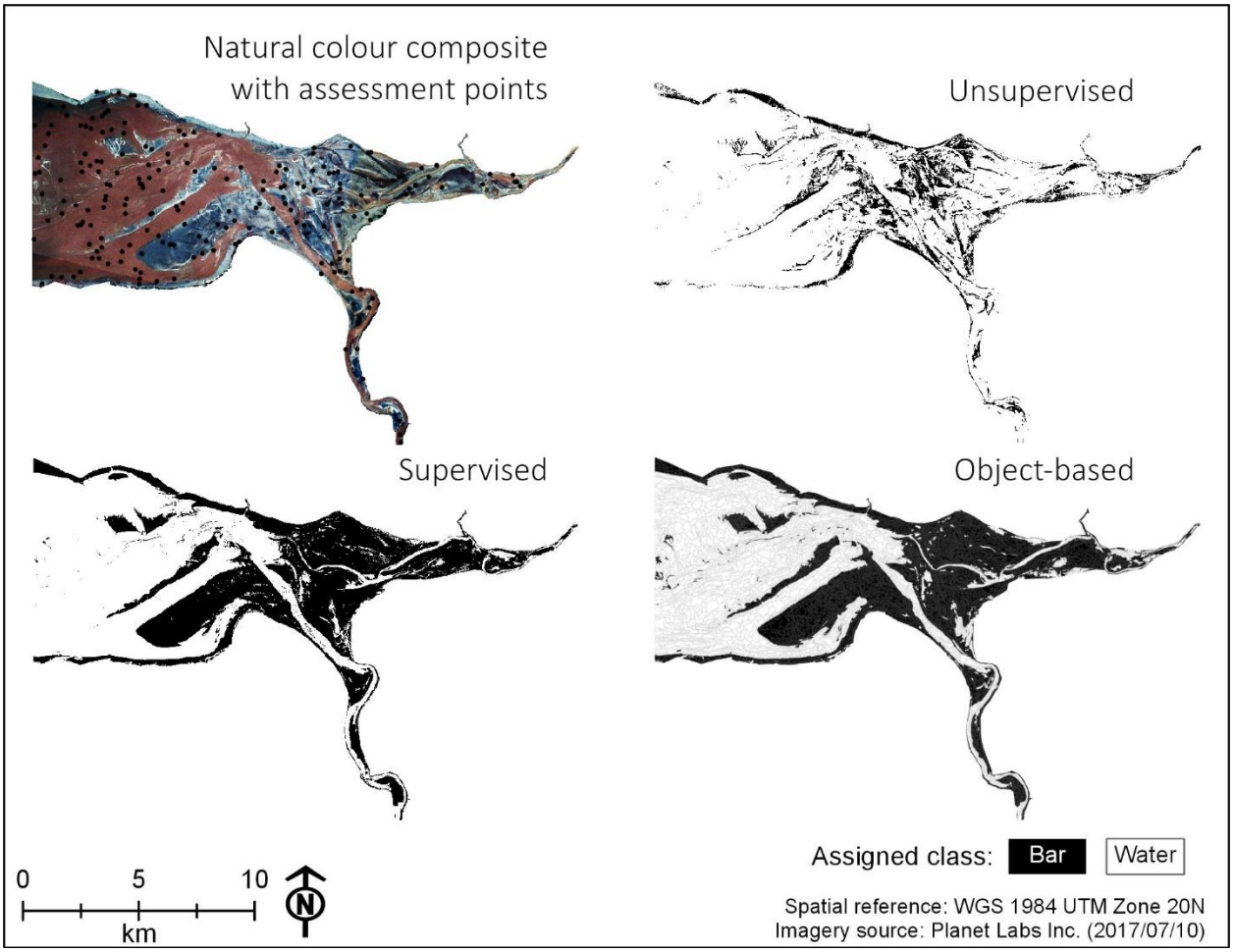

Classification results